

Master's Thesis  
석사 학위논문

Oxygen Reduction Reaction (ORR) Activities of Pt-Ni  
Alloy Nanoparticles Supported on Graphene

Wonkyo Suh (서 원 교 徐 源 教)

Department of Energy Systems Engineering

에너지 시스템 공학 전공

**DGIST**

**2013**

Master's Thesis  
석사 학위논문

Oxygen Reduction Reaction (ORR) Activities of Pt-Ni  
Alloy Nanoparticles Supported on Graphene

Wonkyo Suh (서 원 교 徐 源 教)

Department of Energy Systems Engineering

에너지 시스템 공학 전공

**DGIST**

**2013**

MS/ES

201124008

서 원 교. Wonkyo Suh. Oxygen reduction reaction (ORR) activities of Pt-Ni alloy nanoparticles supported on Graphene. Department of Energy Systems Engineering. 2013. 62P. Advisor Prof. Sangaraju Shanmugam. Prof. Co-Advisors. Oc Hee Han.

## Abstract

Polymer electrolyte membrane fuel cell (PEMFC) has been studied widely due to its higher energy efficiency than a conventional internal combustion engine by generates electrical energy directly from chemical energy. However, the fuel cells faces lots of challenges to commercialization. Cost reduction and improvement of catalysts activities are two major problems impedes the commercialization. Since costly platinum has been used as a catalyst at both anode and cathode of fuel cells, it is required to decrease amounts of Pt. Alloying Pt with secondary transition metals such as Fe, Co, and Ni can reduce the amount of Pt and leading to the cost reduction. In terms of activities, not only Pt-M (M=Fe, Co, Ni, etc.) alloys but carbon support materials should be considered. Graphite materials such as Valcan carbon XC-72 (VXC) and carbon nanotubes (CNT) have been utilized as a carbon support materials for fuel cells. Moreover, since it discovered, graphene has been widely used as a support for electrocatalysts with different metal nanoparticles because of its specific features like high electro-conductivity, surface area and thermal stability.

In an attempt to develop low cost and highly active oxygen reduction reaction (ORR) catalysts, graphene supported Pt-Ni alloy catalyst was synthesized, and the electrochemical ORR performance was evaluated. Due to the ORR sluggish on cathode side plays an important role in fuel cells performance, it is necessary to improve the ORR activities of electrocatalysts. The ORR activity of Pt-Ni supported on graphene was compared with commercial Pt/C catalyst, and Pt-Ni alloy supported on other carbon support materials such as carbon black (VXC) and carbon nanotube (CNT). Among three different electrocatalysts, Pt-Ni alloy catalyst supported on graphene showed highest ORR activity. All Pt-Ni alloy catalysts were followed the direct 4 electron pathway. Among three catalysts, Pt-Ni/graphene catalyst was observed lowest hydrogen peroxide production. Moreover,

Pt-Ni/graphene catalysts showed highest methanol resistance.

Pt-Ni alloy catalysts were characterized using various physical-chemical techniques, such as scanning electron microscopy, transmission electron microscope, X-ray diffraction, and X-ray photoelectron spectroscopy. The electrocatalytic activity and stability of Pt-Ni alloy catalysts were studied using CV, LSV, RDE and RRDE techniques. Thus, developing Pt-Ni alloy supported on various carbon materials with desired properties of ORR activities will be discussed.

Keywords: Fuel cells, Graphene, Pt-Ni alloy catalysts, Oxygen reduction reaction (ORR)



# Contents

Abstract.....	i
Contents .....	iii
List of tables.....	v
List of figures.....	vi
<b>Chapter 1: Introduction .....</b>	<b>1</b>
1.1. Forewords.....	1
1.2. Objectives of the work .....	3
1.3. Advantages & disadvantages of fuel cells .....	4
1.4. Fundamental principles of the fuel cells systems .....	6
1.5. Various types of fuel cells .....	9
1.6. Studies of carbon allotropes for fuel cell carbon support materials .....	13
1.7. Structure and characteristic of graphene .....	15
1.8. Oxygen reduction reaction (ORR) studies .....	18
1.8.1. Low temperature ORR mechanism .....	18
1.8.2. Oxygen reduction reaction on Pt catalyst surface .....	19
<b>Chapter 2: Experimental .....</b>	<b>20</b>
2.1. Chemicals .....	20
2.2. Synthesis of graphene .....	20
2.2.1. Preparation of graphene oxide .....	20
2.2.2. Chemical reduction of graphene oxide to graphene .....	21
2.3. Surface modification of carbon nanotube (CNT) .....	21
2.4. Preparation of Pt-Ni (1:1) (20 wt % metal loading) alloy catalysts supported on carbon black (Vulcan XC-72), CNT, and graphene .....	22
2.5. Characterization .....	22
2.5.1. Physical characterization .....	22

2.5.2. Elemental characterization .....	23
2.5.3. Electrode preparation and electrochemical measurement .....	23
<b>Chapter 3: Results and Discussion .....</b>	<b>25</b>
3.1. Morphologies and size distribution of Pt-Ni based electrocatalysts .....	25
3.2. Crystalline structure analysis of Pt-Ni based electrocatalysts .....	31
3.3. Chemical and electronic properties of Pt-Ni based electrocatalysts .....	34
3.4. Electrochemical studies of Pt-Ni based electrocatalysts .....	39
3.4.1. Electrochemical surface area .....	39
3.4.2. Oxygen reduction reaction activities of Pt-Ni based electrocatalysts .....	41
3.4.3. Methanol tolerance studies of Pt-Ni based electrocatalysts .....	46
3.4.4. Stability of Pt-Ni based electrocatalysts .....	49
<b>Conclusions .....</b>	<b>51</b>
<b>Reference .....</b>	<b>53</b>
<b>국문 요약문 .....</b>	<b>61</b>
<b>Acknowledgement</b>	

## List of tables

Table 1. Various types of fuel cells and their features.....	12
Table 2. Several properties of graphene.....	17
Table 3. Structural characterization of Pt-Ni/VXC, Pt-Ni/CNT, and Pt-Ni/graphene by XRD measurement.....	32
Table 4. XPS binding energy (eV) and peak area (%) of possible chemical states of Pt and Ni in the Pt-Ni/VXC, Pt-Ni/CNT, and Pt-Ni/graphene catalysts.....	38
Table 5. The value of $Q_H$ and ECSA, of Pt-Ni/VXC, Pt-Ni/CNT, and Pt-Ni/graphene catalysts.....	40
Table 6. Electrochemical analysis of Pt-Ni/VXC, Pt-Ni/CNT, and Pt-Ni/graphene catalysts.....	46
Table 7. ECSA decrement of Pt-Ni/VXC, Pt-Ni/CNT, and Pt-Ni/graphene catalysts by CV.....	49

## List of figures

Fig. 1.	First fuel cell electrochemical experiment by Grove.....	5
Fig. 2.	Composition and system image of (a) Proton exchange membrane fuel cells (PEMFCs) and (b) Direct methanol fuel cells (DMFCs).....	7
Fig. 3.	Structure images of a (a) Polytetrafluoroethylene and (b) Sulphonated fluoroethylene (also called perfluorosulphonic acid PTFE copolymer).....	8
Fig. 4.	Different types of $sp^2$ -like hybridized carbon nanostructures (a) $C_{60}$ : Buckyball fullerene (b) Nested giant fullerenes or graphitic onions (c) Carbon nanotube (d) Nanocones or nanohorns (e) Nanotoroids (f) Graphene surface (g) 3D graphite crystal (h) Haeckelite surface (i) Graphene nanoribbons (j) Graphene clusters (k) Helicoidal carbon nanotube (l) Short carbon chains (m) 3D Schwarzite crystals (n) Carbon nanofoams (interconnected graphene surfaces with channels) (o) 3D nanotube networks, and (p) Nanoribbons2D networks.....	14
Fig. 5.	(a) Lattice structure of graphene and (b) $\sigma$ and $\pi$ orbitals placed on graphene structure Extraordinary properties of graphene.....	15
Fig. 6.	One layer of graphene from graphite and its interlayer distance.....	17
Fig. 7.	SEM images of (a) Pt-Ni/VXC, (b) Pt-Ni/CNT, and (c) Pt-Ni/graphene.....	27
Fig. 8.	(a) TEM image, (b) High-resolution TEM image, and (c) Particle size distribution diagram of Pt-Ni/VXC.....	28
Fig. 9.	(a) TEM image, (b) High-resolution TEM image, and (c) Particle size distribution diagram of Pt-Ni/CNT.....	29
Fig.10.	(a) TEM image, (b) High-resolution TEM image, and (c) Particle size distribution diagram of Pt-Ni/graphene.....	30
Fig. 11.	XRD patterns of the Pt-Ni/VXC, Pt-Ni/CNT, and Pt-Ni/graphene catalysts.....	33
Fig. 12.	XRD patterns of graphite, graphene Oxide, and graphene.....	33
Fig. 13.	X-ray photoelectron survey spectra of Pt-Ni/VXC, Pt-Ni/CNT, and Pt-Ni/graphene.....	35
Fig. 14.	Pt4f XPS spectra of (a) Pt-Ni/VXC, (b) Pt-Ni/CNT, and (c) Pt-Ni/graphene.....	36
Fig. 15.	Ni2p XPS spectra of (a) Pt-Ni/VXC, (b) Pt-Ni/CNT, and (c) Pt-Ni/graphene.....	37
Fig. 16.	Cyclic voltammogram of Pt-Ni/VXC, Pt-Ni/CNT, and Pt-Ni/graphene catalysts in $N_2$ -saturated 0.5 M $H_2SO_4$ with a scan rate of $20\text{ mVs}^{-1}$ at $25^\circ\text{C}$ .....	40
Fig. 17.	RDE traces of (a) Pt-Ni/VXC, (c) Pt-Ni/CNT, and (e) Pt-Ni/graphene and Koutechy-Levich plot of (b) Pt-Ni/VXC, (d) Pt-Ni/CNT, and (f) Pt-Ni/graphene catalysts in $O_2$ -saturated 0.5 M $H_2SO_4$ with a scan rate of $5\text{ mVs}^{-1}$ at room temp.....	43
Fig. 18.	Comparison of ORR activities of Pt/C, Pt-Ni/VXC, Pt-Ni/CNT, and Pt-Ni/graphene catalysts in $O_2$ -saturated 0.5 M $H_2SO_4$ with a scan rate of $5\text{ mVs}^{-1}$ at room temp; rotating speed: 1600 rpm.....	44
Fig. 19.	(a) Mass and (b) Specific activities of Pt-Ni/VXC, Pt-Ni/CNT, and Pt-Ni/graphene catalysts at 0.8 V in a 0.5 M $H_2SO_4$ electrolyte.....	44

Fig. 20.	(a) Percentage of H <sub>2</sub> O <sub>2</sub> formation on the ring and (b) Oxygen reduction curves of Pt-Ni/VXC, Pt-Ni/CNT, and Pt-Ni/graphene catalysts measured by RRDE in O <sub>2</sub> -saturated 0.5 M H <sub>2</sub> SO <sub>4</sub> with a scan rate of 5 mVs <sup>-1</sup> at room temp; rotating speed: 1600 rpm.....	45
Fig. 21.	Liner sweep voltammograms of (a) Pt-Ni/VXC and (b) Pt-Ni/CNT in an O <sub>2</sub> -saturated 0.5 M H <sub>2</sub> SO <sub>4</sub> + 0.5 M CH <sub>3</sub> OH electrolyte with a scan rate of 5 mV s <sup>-1</sup> at room temp; rotating speed: 1600 rpm.....	47
Fig. 22.	Liner sweep voltammograms of (a) Pt-Ni/graphene and (b) Pt-Ni alloy catalysts in an O <sub>2</sub> -saturated 0.5 M H <sub>2</sub> SO <sub>4</sub> + 0.5 M CH <sub>3</sub> OH electrolyte with a scan rate of 5 mV s <sup>-1</sup> at room temp; rotating speed: 1600 rpm.....	48
Fig. 23.	Accelerated stability test of (a) Pt-Ni/VXC, (b) Pt-Ni/CNT, and (c) Pt-Ni/graphene by CV in N <sub>2</sub> -saturated 0.5 M H <sub>2</sub> SO <sub>4</sub> with a scan rate of 50mVs <sup>-1</sup> at room temp.....	50

# Chapter 1: Introduction

## 1.1. Forewords

Industrial revolution in the early 18C has been brought consumption of fossil fuels such as petroleum and coals exponentially. As a result of industrialization, destruction of the environment became serious issues. Renewable energy which is environmentally friendly and economical has been developed to solve these problems and fuel cells is one of the most promising energy technologies for the next generation.

Fuel cells uses hydrogen as a fuel and it can be alternative energy source for the future industry instead of fossil fuels. Also it generates water as a byproduct in combination with oxygen and it leads to a zero carbon society. In other words, fuel cells is ideal energy system since it shows high energy efficiency by generates electrical energy directly from chemical energy.

Since nanosized Platinum catalysts offer several advantages, it has been widely used as electrocatalyst in low temperature polymer electrolyte membrane fuel cells (PEMFCs) for a long time.<sup>1</sup> Pt-based electrocatalysts is the most active catalyst for lots of electrochemical reactions such as both oxygen reduction and hydrogen oxidation in fuel cells.<sup>2</sup> However, limitation in platinum stocks over the world and its price can be one of big issues. The world's platinum reserves have been reported about 28,000 tons. If 100 g of platinum use in 100kW fuel cell vehicles, approximately only 280 million fuel cell automobiles can be produced. The world's total vehicles output per year is generally 60 million, therefore the limited reserves of platinum is a serious problem. Furthermore, the high cost of platinum is a problem to be solved. Unfortunately prices of platinum are also rising due to the rapid depletion of platinum.

To settle these problems, development of novel catalysts which can replace with platinum is important. However, it is a fact that specific solutions are not sought yet. Especially in the field of low temperature fuel cells such as polymer electrolyte membrane fuel cells (PEMFCs) and direct methanol fuel cells (DMFCs), it is difficult to find beyond better catalytic ability of platinum catalyst. Therefore, it should be studied in short term and realistic. Alloying platinum with secondary transition metals can

be one of fundamental solution. It can decrease the loading amounts of Pt catalysts, and enhance the fuel cells performance.

To improve electrochemical activities of Pt-based catalysts, high surface area materials, generally carbons, have been widely utilized in low-temperature fuel cells.<sup>3</sup> The activity of an electrocatalysts can increase when the electrochemical surface area increases. For this reasons, to increase dispersion of metal nanoparticles, carbon substrate with a high surface area is essential.<sup>4</sup>

Carbon nanotube (CNT) and graphene are representative nanomaterials for not only fuel cell carbon substrates, but also many industrial applications. Carbon nanotube (CNT) was first found by Dr. Iijima at the NEC corporation in 1991.<sup>5</sup> Since then, numerous studies and experiments have been carried out. Also graphene was found by Prof. Andre Geim and Konstantin Novoselov at the University of Manchester in 2004. They used adhesive tape to separate isolated 2 dimensional carbon nano planes from graphite and they awarded the Nobel Prize in physics for 2010 in recognition of its merits.<sup>6</sup>

Both carbon nanotube (CNT) and graphene have more outstanding chemical, physical and mechanical properties than those used as conventional platinum catalyst support such as activated carbon or carbon black. Therefore, studies using those carbon nano materials as platinum support have been done.

Still it is necessary to make a lot of effort and research continues on the development of fuel cells. However, it can be one of the most important and precious energy resources by developing with nano technologies.

## 1.2. Objectives of the work

Dependence on expensive platinum catalyst cause adverse affect to both development of fuel cells technologies and commercialization. Therefore, improvement of platinum electrocatalyst ability is required. In addition, improving the ability of the catalyst, and research and application of carbon nano materials as support of electrocatalysts which have distinguished physical, chemical, and mechanical properties should also be concerned.

Oxygen reduction reaction (ORR) plays an important role in the fuel cells system.<sup>7</sup> Research trends of fuel cells electrocatalysts are focused on the cathode, where the oxygen reduction occurs. Enhancement of ORR activities, which is one of the most important phenomenons in fuel cells system, can bring an improvement of fuel cells performance. In other word, development of electrocatalysts which can enhance ORR in fuel cell systems is necessary.

In order to improve activities and to decrease the cost of fuel cells, Pt alloy catalyst with a non-noble metal can be one of a successful strategy.<sup>8</sup> It has been shown that ORR of platinum electrocatalyst can be improved by alloying with secondary transition metals such as Cu, Cr, Fe, and Ni for fuel cells catalyst.<sup>9,10</sup>

To further enhance of electrocatalytic activity of alloy catalyst, various carbon support materials, such as carbon black, carbon nanotube have been applied. Also graphene has been used as a support material for fuel cell electrode due to its high conductivity, large surface area, thermal stability and physical strength.

In this thesis, platinum and nickel alloy electrocatalysts supported on different carbon materials (Vulcan XC-72, CNT, graphene) will be studied to reduce the amount of platinum and improve oxygen reduction reaction activity as the fuel cells catalyst. Other fundamental properties of Pt-Ni alloy electrocatalysts, such as stability and methanol tolerance in acidic solution will also be measured. Furthermore, we can determine through rotating disk electrode (RDE) and rotating ring disk electrode (RRDE) techniques whether it follows 4-electron reaction or peroxide pathway during ORR.

### 1.3. Advantages & disadvantages of fuel cells

It might be a surprise to a lot of people that the first fuel cells technology was invented and applied about more than 100 years ago. The first experiment of fuel cells in history was made by a UK Amateur scientist, Sir William Grove in 1839.<sup>11</sup> The basic principle of hydrogen fuel cell is shown in Fig. 1. The First fuel cell was operated by electrolysis of water. Hydrogen and oxygen were separated when electric current pass through the water. By reverse reaction of electrolysis, the hydrogen and oxygen were combined again and the electric current was generated. From the early 1960s in the United States and the Soviet Union, research and development of the fuel cells have been carried out for both military and scientific purposes in earnest. By definition of the fuel cells exactly, it is the cell that direct current provided when chemical energy of fuel conversed directly into electric energy. There are several specific features of the fuel cells.<sup>12</sup>

#### A. High efficiency

To generate electricity, without convert process from thermal energy into mechanical energy, the efficiency of fuel cells is about 10 to 20 % higher than the internal combustion engines.<sup>13</sup>

#### B. Cogeneration system

Due to its produced heat from reaction process, it is available to generate both electricity and thermal energy simultaneously from fuel cell system; it is suitable for cogeneration system. Approximately 40 to 50 % of inserted fuels are utilized as electrical energy and about 40 % can be used as thermal energy. In other words, fuel cell system is able to consume comprehensively 80 to 90 % of effective energy.<sup>14</sup>

#### C. Simplicity

The operation system of the fuel cell is simpler than other energy conversion devices. Whereas established energy systems such as thermal power generations are more complicated than fuel cell

systems, since it require generator connected a steam turbine to produce electricity from combusted fossil fuels.<sup>15</sup>

#### D. Clean industrial

Fuel cell system is one of the environmental friendly technologies. When hydrogen is supplied as fuel into the system, the main by-product of fuel cell reaction is pure water. It suggests that pollutions such as sulfur oxides, nitrogen oxides, and dust from exhaust gas system are very low. However, production of carbon dioxides during the fuel reforming process is inevitable.<sup>16</sup>

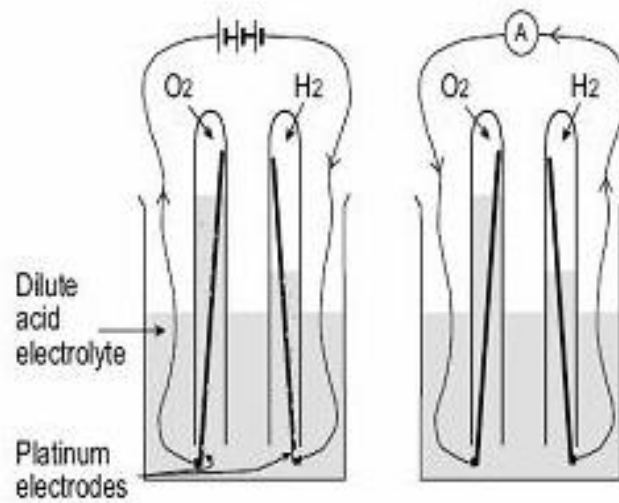
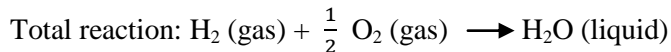
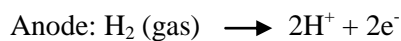


Fig. 1. First fuel cell electrochemical experiment by Grove.<sup>12</sup>

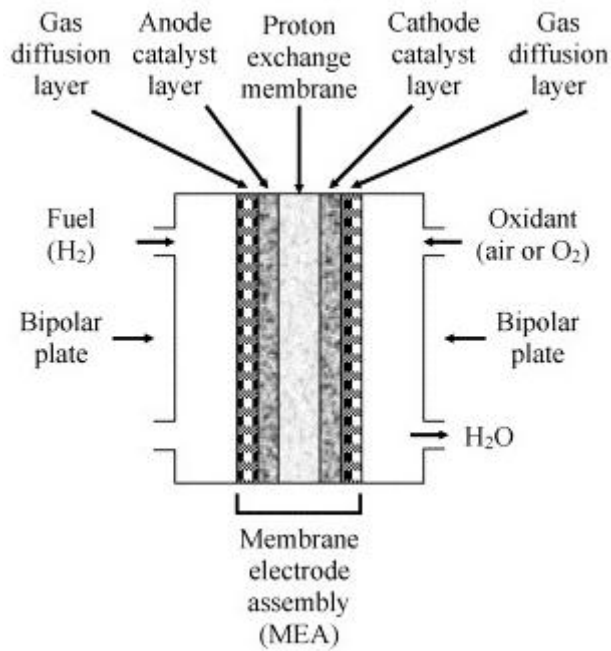
#### 1.4. Fundamental principles of the fuel cells system

Fig. 2 shows the composition and the reaction principles of polymer electrolyte membrane fuel cells (PEMFCs) and direct methanol fuel cells (DMFCs). As shown in Fig. 2, in the PEMFCs, hydrogen flows from the anode as fuel and oxygen (or air) is inserted at the cathode. And a fluorinated ion exchange membrane is sandwiched between anode and cathode electrodes. Hydrogen from anode provides protons and electron to the cathode. Protons directly passing through, the fluorinated ion exchange membrane, electrolyte and the electrons are flow by external circuit from anode to cathode. Both protons from the anode and electrons from external circuit are recombined with oxygen at the cathode. Finally, water is produced as a product. The reactions at the anode and cathode are as follows:

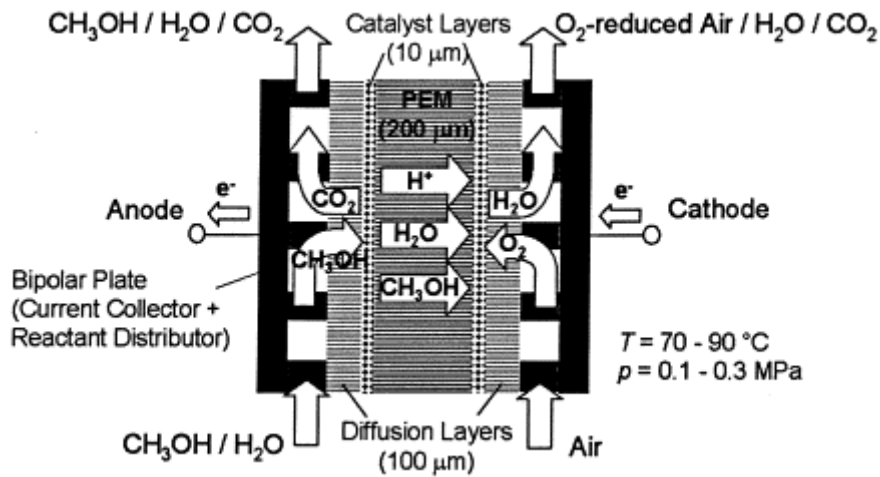


Electrocatalysts of polymer electrolyte membrane fuel cells (PEMFCs) should be concerned about activation with regard to both hydrogen and oxygen. Moreover, chemical durability is also important since the fuel cell systems are operated at high voltage and under strong acidic condition.

Not only electrocatalysts but polymer electrolyte membrane has its own properties and specific features. Most commonly used proton conductive membranes are sulphonated fluoropolymers, Nafion, from Dupon generally. Fig. 3 shows simple structure of (a) polytetrafluoroethylene and (b) sulphonated fluoropolymers. As shown in Fig. 3, (a) the strong bond connection between the carbon and the fluorine is able to enhance durable and chemical resistant. (b) Hydrogen ions choose a well hydrated region for ion transfer path. It shows also hydrophilic properties partially because of  $\text{HSO}_3$  group. And hydrogen ions choose well hydrated region for ion transfer path.

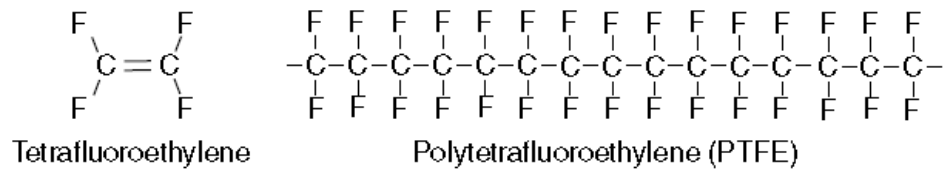


(a)

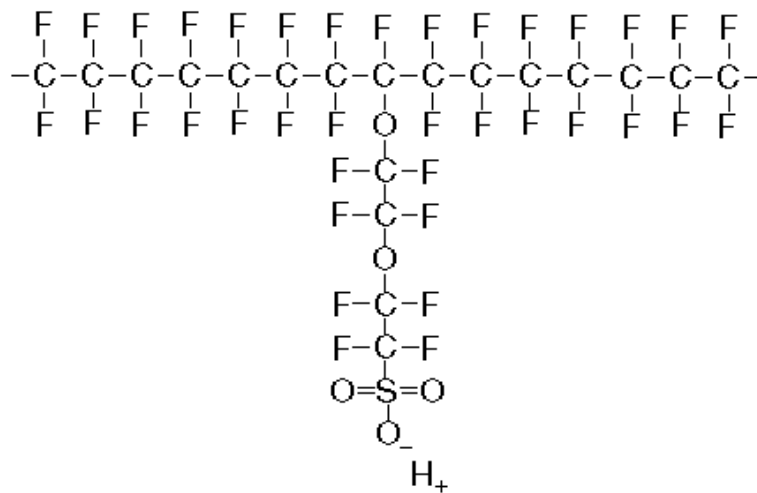


(b)

Fig. 2. Composition and system image of (a) Proton exchange membrane fuel cells (PEMFCs) and (b) Direct methanol fuel cells (DMFCs).<sup>17,18</sup>



(a)



(b)

Fig. 3. Structure images of a (a) Polytetrafluoroethylene and (b) Sulphonated fluoroethylene (also called perfluorosulphonic acid PTFE copolymer).<sup>12</sup>

## 1.5. Various types of fuel cells

Fuel cells can be divided into several different types according to their various electrolytes, fuels, and reactants. The following studies indicate different features of each of the fuel cell types, what kinds of systems apply to each fuel cell, and how each difference in operating features, materials, and applications can be utilized in numerous industrial fields.<sup>14</sup>

### A. Alkaline fuel cells (AFCs)

Alkaline fuel cells use alkali such as potassium hydroxide as an electrolyte. Pure hydrogen flows as fuel from the anode and oxygen is used as an oxidant. Since it is a low temperature fuel cell, its operating temperature at atmosphere is 60 to 120 °C. In AFC nickel was chosen as an electrocatalyst due to it is low-cost materials for the electrodes. Storage of hydrogen and effective removal of carbon dioxide is one of the most important factors in the AFC system.

### B. Phosphoric acid fuel cells (PAFCs)

Phosphoric acid ( $\text{H}_3\text{PO}_4$ ) shows high in thermal, chemical, and electrochemical stability and low volatility (about 150 °C). Phosphoric acid is the only inorganic acid fuel cell electrolyte. Also it has high  $\text{CO}_2$  tolerance to mixture of fuel and oxidant. Almost 70% pure hydrogen is used as fuel in PAFC and platinum or platinum alloys supported on carbon black can be used as the electrode. Original efficiency of PAFC is approximately 40 to 50 %. However, using the heat from fuel cell reaction, it can be improved to more than 70 %.

### C. Molten carbonate fuel cells (MCFCs)

Molten carbonate fuel cells (MCFCs) is a high temperature fuel cell, and carbonic acid gas is circulated as fuel. The electrolyte of the MCFCs is a molten mixture of alkali metal carbonates. At high operating temperatures (normally 600 to 700°C) alkali metal carbonates show high ion conductivity that makes it possible to pass carbonate  $\text{CO}_3^{2-}$  ions. Most different feature of MCFCs is

that it requires carbon dioxide and carbon dioxide plays important roles in MCFC systems. It is transformed to carbonate ions and it delivers ions between the anode and cathode. Also reforming of hydrocarbon gas can be proceeded by inner heat of fuel cell stack. In results of self reforming, cost can be reduced almost 30 %.

#### D. Solid oxide fuel cells (SOFCs)

Solid oxide fuel cells (SOFCs) consist all cell components with complete solid state system which uses oxide ion conducting ceramic materials as the electrolyte.<sup>19</sup> Like Molten carbonate fuel cells (MCFCs), it is a high temperature fuel cell whose operating temperature is about 800 to 1000 °C. A material for anode is a Ni-zirconia cermet, and it displays high electronic conductivity and stability of chemical reducing conditions. Strontium (Sr) doped lanthanum manganate is most general cathode material for SOFCs.<sup>20</sup> Electrochemical oxidation reaction of hydrogen and carbon monoxide in SOFCs takes place spontaneously at 1000 °C so that fuel can be reformed without any catalyst.

#### E. Polymer electrolyte membrane fuel cells (PEMFCs)

Solid polymer electrolyte is applied as the membrane in PEMFC. Hydrogen and oxygen are inserted from the anode and the cathode respectively. And it reacts as a fuel and oxidant. Similarly to membrane using Phosphoric acid fuel cell (PAFC) systems, it uses platinum for catalyst. It also has corrosion problem of metal catalysts in acid condition, and it leads to low durability. Even though the PEMFC developed almost a decade later, it has been widely studied because of its low operating temperature and high power density.

#### F. Direct methanol fuel cells (DMFCs)

Direct methanol fuel cells (DMFCs) uses methanol as fuel and through direct electrochemical reaction of methanol, it generates heat and electricity. Similar to PEMFCs it is a low temperature fuel cell and the system is relatively simple because it does not require the fuel reformer. Moreover, the DMFCs is suitable for portable devices such as lap-top and cellular phone.

Table. 1. Various types of fuel cells and their features

<u>Type of fuel cells</u>	<u>AFCs</u>	<u>PAFCs</u>	<u>MCFCs</u>	<u>SOFCs</u>	<u>PEMFCs</u>
Electrolyte	KOH	H <sub>3</sub> PO <sub>4</sub>	(Li, K) <sub>2</sub> CO <sub>3</sub>	ZrO <sub>2</sub>	Polymer membrane
Charge carrier	OH <sup>-</sup>	H <sup>+</sup>	CO <sub>3</sub> <sup>2-</sup>	O <sup>2-</sup>	H <sup>+</sup>
Anode	Pt/C	Pt/C	Ni + 10wt% Cr	Ni + (Zr, Y)O <sub>2</sub>	Pt/C
Cathode	C	C	NiO	(La, Sr)MnO <sub>3</sub> , LaCoO <sub>3</sub>	Pt/C
Operation temperature	50 to 200 °C	150 to 200 °C	600 to 700 °C	600 to 1000 °C	30 to 100 °C
Fuels	H <sub>2</sub>	Natural gas	Natural gas, H <sub>2</sub> , CO	Natural gas, Petroleum	H <sub>2</sub>
Application	Military and space	transportation	Large generation	Stationary, transportation	Small stationary, transportation

## 1.6. Studies of carbon allotropes for fuel cell carbon support materials

Carbon is one of the most important elements for not only composition of life but also material of electrochemical applications such as batteries and fuel cells. In addition, it has been utilized for the storage of energy especially. During the last several years numerous studies has been carried out and focused on the uses of carbon as electrode materials due to its accessibility, easy processability, and low cost.<sup>21</sup>

Elemental carbon was believed that it has existed only two conformation, diamond and graphite, which consist of  $sp^3$  and  $sp^2$  hybridized carbon atoms respectively.<sup>22</sup> Both forms have especial physical, chemical, and mechanical properties as mentioned before. However, in 1985 fullerenes was observed for the first time by Kroto et al.<sup>23</sup> It also called Buckyball that it consists of 60 carbons and it formed similar with soccer ball. Carbon atoms in fullerene can make not only hexagonal but heptagonal and pentagonal structures. Depends on the number of carbon atoms, it has been called  $C_{60}$  and  $C_{70}$ . This new molecular form of carbon is soluble in organic solvents and other atoms can be trapped inside fullerenes to form endohedral fullerenes. Moreover, it has extraordinary property that it is non-toxic to the human body so that it also can be applied to medical fields. After discovering fullerenes, investigation of carbon materials was accelerated.

Similarly with graphene, carbon nanotube (CNT) is also one of the great discoveries in 20 century. It is a cylindrical  $sp^2$  hybridized carbon nanostructure. Depending on the rolled layer, CNTs are categorized into single-walled nanotubes (SWNT) and multi-walled nanotubes (MWNT). Both SWNT and MWNT also show great physical and mechanical properties as graphene. Because of their good thermal conductivity, high electron mobility, and mechanical strength it can be a great candidates of materials for fuel cells electrode. Furthermore, especially catalysts field, many kinds of researches were already carried out with nanotubes. Fig. 6 shows that different types of carbon nanostructures

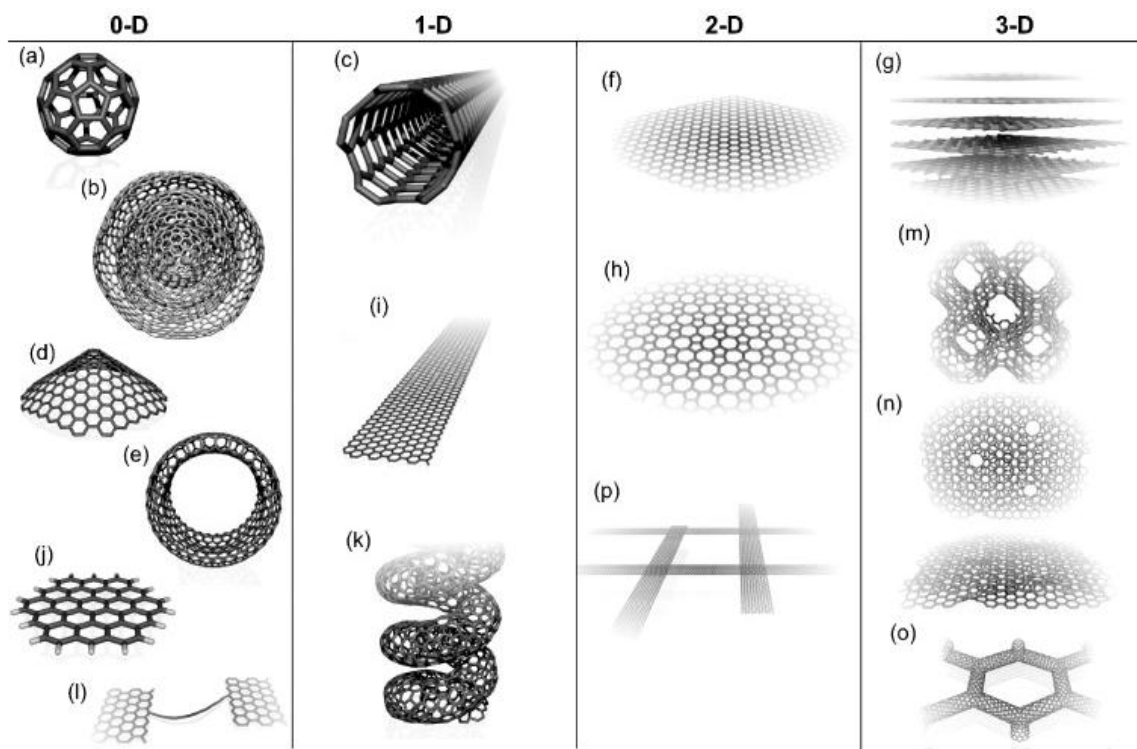


Fig. 4. M. Terrones et al. suggest different types of  $sp^2$ -like hybridized carbon nanostructures (a)  $C_{60}$ : Buckyball fullerene (b) Nested giant fullerenes or graphitic onions (c) Carbon nanotube (d) Nanocones or nanohorns (e) Nanotoroids (f) Graphene surface (g) 3D graphite crystal (h) Haeckelite surface (i) Graphene nanoribbons (j) Graphene clusters (k) Helicoidal carbon nanotube (l) Short carbon chains (m) 3D Schwarzite crystals (n) Carbon nanofoams (interconnected graphene surfaces with channels) (o) 3D nanotube networks, and (p) Nanoribbons 2D networks (from : M. Terrones et al., *Nano Today* **5**, 351-372).<sup>24</sup>

## 1.7. Structure and characteristic of graphene

Graphene has received considerable interest in many research field due to its exceptional physical and chemical properties.<sup>25</sup> It has been investigated in many applications, such as sensors, batteries, solar cells, and fuel cells.<sup>26</sup> It can be utilized as fuel cell materials for electrode because of its unique and extraordinary features like extensive nanostructure, high surface area <sup>27</sup>, superior thermal conductivity<sup>28</sup> and electronic conductivity<sup>29</sup>, and mechanical strength.<sup>30</sup>

Graphene is a single nano sheet of graphite that consisted of only carbon. One layer of graphene can be separated from graphite using chemical functionalization <sup>31</sup>, thermal exfoliation <sup>32</sup>, mechanical cleavage.<sup>33</sup> Naturally, carbon has  $2s$  and  $2p$  orbital and each orbital include 2 electrons respectively. These four electrons in carbon make different kinds of  $sp$ -hybridized orbital. Every carbon atom in graphene is bounded with neighbored three other carbon atoms as  $sp^2$  hybridization.<sup>34</sup> As shown in Fig. 4 (b) there are three  $\sigma$  orbitals on the one carbon atom in a layer of graphene and one  $\pi$  orbital along with vertical direction. When chemical sorption occurs on graphene, one  $\pi$  bond breaks and it produces another one  $\sigma$  orbital. In other words, change from  $sp^2$  to  $sp^3$  hybridization is the major mechanism of chemical absorption of graphene.

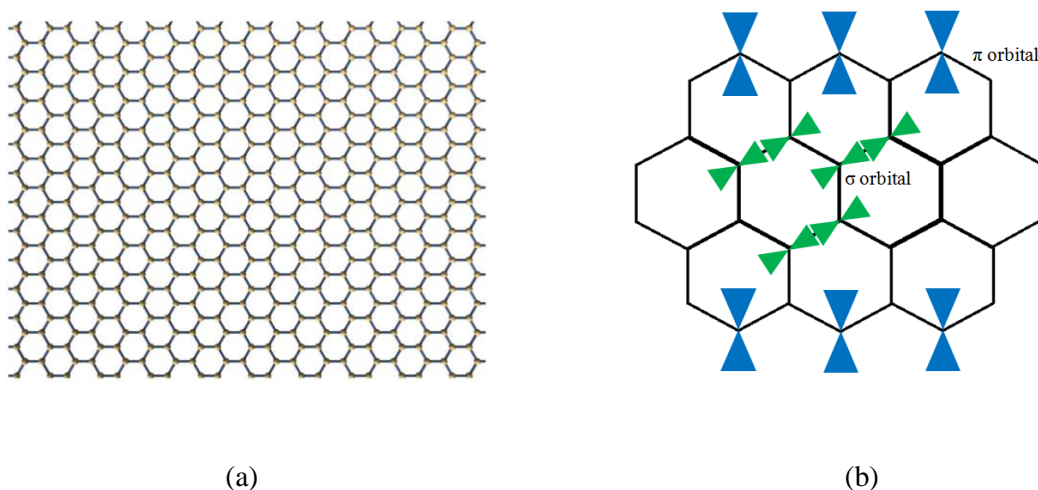


Fig. 5. (a) Lattice structure of graphene and (b)  $\sigma$  and  $\pi$  orbitals placed on graphene structure  
Extraordinary properties of graphene.

Graphene has unique  $\pi$ -stacked hexagonal structure from graphite with 0.3 nm of interlayer distance (Fig. 5.) and thickness of one layer of graphene is almost a atom size, it includes several extraordinary properties.<sup>35</sup> Most of all features are advanced than the other carbon allotropes.

The thermal properties of graphene have been found near 5,000 W/mK which is higher than experimental measured value of both carbon nanotubes and diamond. It was studied through a suspended graphene nano layer that obtained by mechanical exfoliation.<sup>36</sup>

Mechanical strength of a single graphene layer shows about 200 times higher breaking strength than steel with Young`s modulus of 1 TPa and fracture strength of 125 GPa.<sup>30</sup> Moreover, Xin Z et al reported that tensile strength was improved almost 150% according to low loading of graphene (1.8 vol %) with poly (vinyl alcohol) (PVA).<sup>37</sup>

Graphene also has ultrahigh electron mobility. Thermal vibration of atom in graphene determines electron mobility and it has been reported that the values of mobility is approximately 200,000 cm<sup>2</sup>/Vs.<sup>38</sup> In case of Si it was measured about 1,400 cm<sup>2</sup>/Vs. In addition, electron mobility decides the switching speed of electronic devices and the graphene can be a superior candidate for transistor which needs fast switching speed. Surface area of one single layer graphene can be measured by Brunauer-Emmett-Teller (BET) technique<sup>39</sup> and it was 2,630 m<sup>2</sup>/g of surface area, which is almost twice surface area compared with multi wall carbon nanotube (MWCNT) (~1,500 m<sup>2</sup>/g).

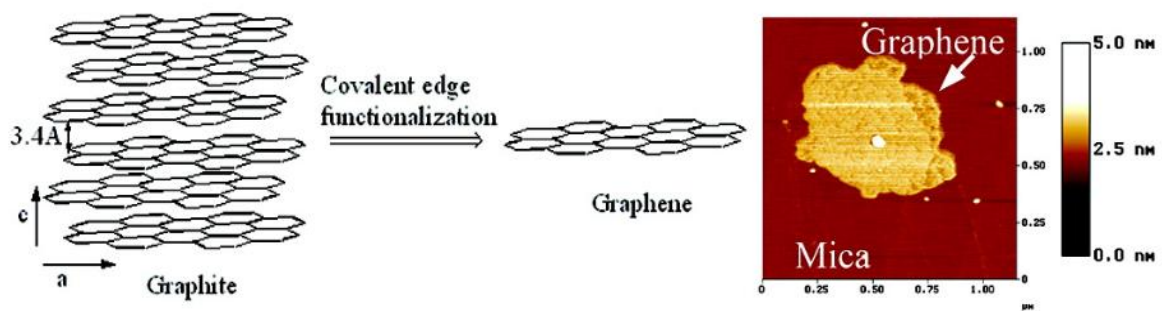


Fig. 6. One layer of graphene from graphite and its interlayer distance.<sup>35</sup>

Table. 2. Several properties of graphene

Properties	Graphene
Electron mobility	200,000 cm <sup>2</sup> /Vs
Thermal conductivity	5,000W/mK
Young`s modulus	1 TPa
Surface area	2,630 m <sup>2</sup> /g
Mean free path	~1.0 μm

## 1.8. Oxygen reduction reaction (ORR) studies

### 1.8.1. Low temperature ORR mechanism

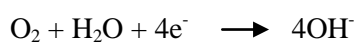
Low temperature reduction of oxygen was studied as a part of low temperature fuel cells research throughout the 1960s and '70s. Especially, high overpotential that occur during oxygen reduction make difficult to commercialization of low temperature fuel cells. In this regard, development of novel catalyst has been one of the most important challenges to increase ORR.

Electrochemically, ORR is significantly affected by the electrode surface and adsorbents. For this reason, materials of electrodes, catalyst crystal face characteristic, catalyst surface modification, and electrolyte studies have been carried out. In other words, this reaction has been studied on many materials and in electrolytes.<sup>40</sup> Platinum is representative catalyst for fuel cells and it shows very strong activities in the acid electrolyte. In additions, the Damjanovic mechanism was reported and accepted widely.<sup>41,42</sup>

ORR on cathode is determined by many variable factors such as various kinds of catalysts and electrolytes. ORR follow two reaction pathways both in acidic and alkaline media. The one is direct 4-electron pathway and another is peroxide pathway via two electron pathway.

#### i. Direct 4-electron pathway

##### Alkaline media:

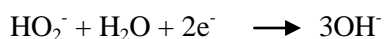
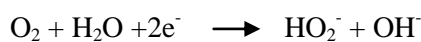


##### Acidic media:

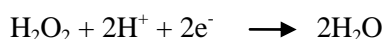
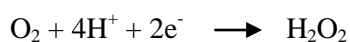


ii. Peroxide pathway

Alkaline media:



Acidic media:



### 1.8.2. Oxygen reduction reaction on Pt catalyst surface

Oxygen reduces directly to  $\text{OH}^-$  or  $\text{H}_2\text{O}$  with 4-electron reaction and peroxide can be involved as intermediate. However, the formation of hydrogen peroxide at the 4-electron pathway can be either extremely low or it does not generated in the electrolyte. It is known that intermediated such as O, OH, and OOH species are absorbed on Pt surface when ORR is carried out. Moreover mixed potential is occurred through the Pt surface oxide formation such as Pt-O and Pt-OOH. High absorption of OH species on the Pt surface leads to decrease in the active sites for the  $\text{O}_2$  adsorption. This means that it causes decline of ORR activities.

The adsorption of OH on Pt surface can be reduced by alloying Pt with secondary transition metals such as Fe, Co, and Ni. Essentially Pt has high binding energy between Pt surface and oxygen from oxygenated species such as  $\text{O}_2$ , O, OH, and OOH. D-band center of pure Pt surface is placed above of Fermi-level compared to that of the Pt-M (M = secondary transition metals such as Fe, Co, and Ni) alloy catalyst. When Pt-M alloy is formed, the electron transfer is occurred from transition metal to Pt. As a result of that, the band width changes broad and d-band center of Pt downshift relative to Fermi-level.

## Chapter 2: Experimental

### 2.1. Chemicals

Graphite, Chloroplatinic acid ( $\text{H}_2\text{PtCl}_6 \cdot 6\text{H}_2\text{O}$ ,  $\geq 37.50$  % Pt basis), potassium persulfate ( $\text{K}_2\text{S}_2\text{O}_8$ , 99 %), phosphorus pentoxide powder ( $\text{P}_2\text{O}_5$ ,  $\geq 98.0$  %), sulfuric acid ( $\text{H}_2\text{SO}_4$ , 95 – 98%) were obtained from Aldrich. Nickel chloride ( $\text{NiCl}_2 \cdot 6\text{H}_2\text{O}$ , 98 %) was obtained from Kanto Chemicals. Sodium borohydride ( $\text{NaBH}_4$ ,  $\geq 98.0$  %), sodium hydroxide ( $\text{NaOH}$ ,  $\geq 98.0$  %), hydrogen peroxide ( $\text{H}_2\text{O}_2$ ,  $\geq 34.5$  %), potassium permanganate ( $\text{KMnO}_4$ ,  $\geq 99.3$  %), sodium chloride ( $\text{NaCl}$ ,  $\geq 99.0$  %) were purchased from Samchun Chemicals. Hydroiodic acid (HI, 55 – 58 %) was purchased from Junsei Chemicals. Nitric acid ( $\text{HNO}_3$ , 60%) was obtained from Daejung Chemicals

### 2.2. Synthesis of graphene

#### 2.2.1. Preparation of graphene oxide

Graphene oxide was prepared based on the Hummers method.<sup>43</sup> 1 g of graphite powder was ground with 50 g of sodium chloride ( $\text{NaCl}$ ) until becomes fine powder. The gray powder was washed with distilled water several times and washed with ethanol finally. Dried filtrated graphite at 80 °C oven and collected remains. Reflux graphite powder at 80 °C in oil bath with sulfuric acid ( $\text{H}_2\text{SO}_4$ , 4 mL), potassium persulfate ( $\text{K}_2\text{S}_2\text{O}_8$ , 0.84 g), and phosphorus pentoxide powder ( $\text{P}_2\text{O}_5$ , 0.84 g) for 4.5 h. Then it was cooled down to room temp. for 10 to 20 minute. After that 167 mL of distilled water was added and it was stirred overnight with 500 rpm at ambient temperature. The solution was filtrated and washed with distilled water several times. Washed remain solid was dried at 80 °C oven. After dried it was stirred with 40 mL of  $\text{H}_2\text{SO}_4$  and potassium permanganate ( $\text{KMnO}_4$ , 5g) was added slowly in ice bath. Then 84 mL of distilled water was mixed and it was stirred at 35 °C in oil bath for

2 h. 167 mL of distilled water and hydrogen peroxide ( $\text{H}_2\text{O}_2$ , 10mL) was added and it was stirred for 0.5 h in ice bath. Color of solvent was changed rapidly from black to dark yellow. Finally, the solvent was centrifuged several times at 12000 rpm for 20 min until the pH adjusted to 7. Centrifuged solid was dried at 80 °C oven overnight.

### **2.2.2. Chemical reduction of graphene oxide to graphene**

1 g of Graphene oxide was dispersed in 375 mL of acetic acid ( $\text{CH}_3\text{COOH}$ ). After sonication, the solvent was stirred until the solution becomes clear. After stirred enough, 20 mL of hydroiodic acid (HI) was added and it was stirred at 40 °C for 40 h with constant stirring speed. Then the solution was filtrated with 250 mL of saturated sodium bicarbonate ( $\text{NaHCO}_3$ ) and 10 mL of acetone. Finally it was dried at 30 °C for 7 h in the vacuum oven.

### **2.3. Surface modification of carbon nanotube (CNT)**

Carbon nanotube (CNT) surface was modified with functional group such as O, OOH, and OH to facilitate the adsorption of metal catalysts. 0.5 g of CNT was dispersed in each 20 mL of  $\text{H}_2\text{SO}_4$  and nitric acid ( $\text{HNO}_3$ ). The solution was refluxed at 120 °C for 5 h. After reflux the solvent, it was stirred with 200 mL of distilled water at room temp. for 3 h. finally it was filtrated and washed several times with distilled water. The contents were dried at 80 °C oven.

## **2.4. Preparation of Pt-Ni Pt-Ni (1:1) (20 wt % metal loading) alloy catalysts supported on carbon black (Vulcan XC-72), CNT, and graphene**

Three different carbon materials (Vulcan XC-72, CNT, and graphene) were used as support of Pt-Ni alloy catalyst and synthesis procedure was same except carbon supports. In this section a typical synthesizes of Pt-Ni supported graphene was discussed. Similar procedure was used to prepare other catalysts

0.1 g of graphene was dispersed in 20 mL of anhydrous ethanol and the solution was sonication for 1 h. Chloroplatinic acid ( $\text{H}_2\text{PtCl}_6 \cdot 6\text{H}_2\text{O}$ , 0.0265 g) and nickel chloride ( $\text{NiCl}_2 \cdot 6\text{H}_2\text{O}$ , 0.04g) as metal precursor were dissolved in distilled water. After that, it was dropwise to graphene dispersed ethanol solvent under sonication. 1M of sodium hydroxide ( $\text{NaOH}$ , 400  $\mu\text{L}$ ) was added to adjust pH around 13. Then sodium borohydride ( $\text{NaBH}_4$ , 0.5 g) as a reducing agent was also added slowly. The solution was stirred for 1 h at the room temp. under  $\text{N}_2$  atmosphere. Finally it was centrifuged with distilled water at 12000 rpm for 20 min several times to adjust pH 7. And the Pt-Ni alloy catalyst supported on graphene slurry was dried 80 °C oven. Also heat treatment was carried out at 200 °C under  $\text{H}_2$  and Ar mixed gas to reduce metal ion to metal nanoparticles and also eliminate impurities.

## **2.5. Characterization**

### **2.5.1. Physical characterization**

The morphologies and size distributions of Pt-Ni alloy catalysts were measured by scanning electron microscopy (SEM) and high resolution-transmission electron microscopy (HR-TEM).

Structure studies such as degree of alloying and crystallite size of Pt-Ni alloy nanoparticles supported on VXC, CNT, and graphene was carried out by X-ray diffraction (XRD) measurement. XRD was performed with Copper K- $\alpha$  radiation (wavelength = 1.54 Å) at 40kV and 30 mA. The

diffraction patterns of Pt-Ni alloy catalysts supported on carbon materials were obtained in  $2\theta$  ranges from 20 to 90°. The clean powder samples were directly placed on XRD sample holder and the scans were carried out with a step size of 0.026. Lattice parameters and particle size were calculated by using Bragg's law and Scherrer's formula respectively.<sup>44</sup>

### **2.5.2. Elemental characterization**

The reactivity of given metal can be modified by alloying.<sup>45</sup> Also the ORR activities of samples can be affected considerably compared to pure Pt catalyst. For these reasons, Surface elemental composition and the oxidation state of Pt-Ni alloy catalysts were investigated by analysis of the X-ray photoelectron spectra (XPS). XPS data were obtained from a monochromated Al K $\alpha$  source ( $h\nu = 1486.6$  eV). In addition it was operated at 150W with 15kv of X-ray energy.

### **2.5.3. Electrode preparation and electrochemical measurement**

The catalyst slurry was prepared to coat onto a polished glassy carbon (GC) electrode. 5 mg of catalyst powder was dispersed in 4 mL of distilled water, 1 mL of isopropyl alcohol (IPA) and 20  $\mu\ell$  of Nafion solution (5 wt.%). The ink was sonicated for 0.5 h. 10  $\mu\ell$  of suspended catalyst ink was dropped onto GC electrode and dried in room temp.

Cyclic voltammogram (CV) (3 mm diameter) was performed in the potential range of 0-1.2 V VS. RHE under nitrogen saturated 0.5 M H<sub>2</sub>SO<sub>4</sub> electrolyte to determine the Pt electrochemical surface area (ESA) and accelerated stability test (AST). CV was carried out at a scan rate of 20 mV s<sup>-1</sup> for ESA measurement and 50 mV s<sup>-1</sup> for AST. Furthermore, the ORR activities, methanol tolerance, and durability test was carried out with rotating disk electrode (RDE) (3 mm diameter). GC electrode of RDE, Pt wire, and saturated calomel electrode (SCE) was used as working, counter, and reference electrode respectively. RDE was measured in oxygen saturated 0.5 M H<sub>2</sub>SO<sub>4</sub> electrolyte at a scan rate

of 5 mV s<sup>-1</sup>.

Rotating ring-disc electrode (RRDE, 4 mm diameter) studies were also carried out to determine effect of hydrogen peroxide production. RRDE experiments were performed under saturated 0.5 M H<sub>2</sub>SO<sub>4</sub> electrolyte with 1600 rpm rotating speed. The disc electrode potential was scanned from 0.2-1.2 V vs. RHE at a scan rate of 5 mV s<sup>-1</sup>, the ring electrode potential was held at 1.2 V vs. RHE in order to obtain the oxidation current of H<sub>2</sub>O<sub>2</sub> into O<sub>2</sub>.<sup>46</sup>

## Chapter 3: Results and Discussion

### 3.1. Morphologies and size distribution of Pt-Ni based electrocatalysts

SEM images of Pt-Ni alloy catalysts supported on carbon black (Vulcan XC-72, VXC), carbon nanotube (CNT), and graphene are shown in Fig. 7. The overall morphologies of three different carbon support materials show clearly differences. It was observed that VXC particles were distributed in a large range and the particle size of carbon black is less than 100 nm (Fig. 7(a)). CNTs demonstrated as tangled tubes-like structures with diameters of approximately 20 to 40 nm.

Graphene, a single layer of graphite, revealed a different morphology compared to VXC and CNT. As shown in Fig. 7(c), graphene was observed as a crumpled, paper-like structure. Moreover, it can be observed that Pt-Ni alloy catalyst-supported graphene is composed of only a few layers of graphene. Clear images of both Pt-Ni catalysts distribution and graphene single nano sheets are generally difficult to identify from SEM analysis because the size of Pt-Ni particles in this studies are less than 10 nm and the thickness of graphene is about 1 to 2 nm.

The morphology and dispersion of three samples were also examined by TEM measurement. Figs. 8, 9, and 10 show that Pt-Ni nano particles were deposited uniformly onto support materials. Figs. 8, 9, and 10 (a) clearly show the distribution degree of nanoparticles and the different structures of carbon support materials. Also, every sample has crystalline structures, as illustrated in Figs. 8, 9, and 10 (b). The lattice fringes of each sample were measured by high-resolution TEM (HRTEM), and the estimated lattice fringe distance was 0.22 nm, 0.17 nm, and 0.27 nm, respectively, for Pt-Ni/VXC, Pt-Ni/CNT, and Pt-Ni/graphene. In addition, particle size was evaluated as shown in Fig. 8, 9, and 10 (c). The Pt-Ni alloy nanoparticles sizes in the sample of 20 wt% Pt-Ni/VXC, Pt-Ni/CNT, and Pt-Ni/Graphene were measured as between  $2.5 \pm 0.5$  and  $4.5 \pm 0.5$  nm. The largest particle size measured about 5.7 nm and the smallest one was approximately 1.7 nm.

In addition, ORR activities of Pt based electrocatalysts can be decreased if particle aggregation occurs. However, it was observed that such an aggregation of metal nanoparticles on the carbon

support materials did not occur. Therefore, it can be assumed that aggregation of the Pt-Ni alloy nanoparticles was not affected by degeneration of electrocatalyst activities.

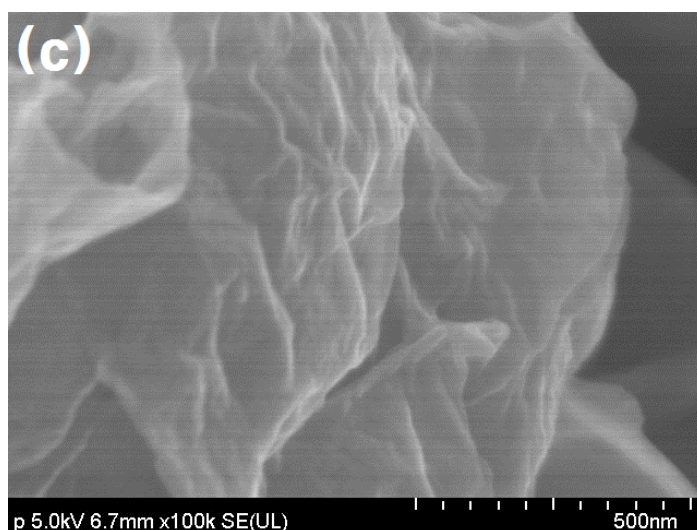
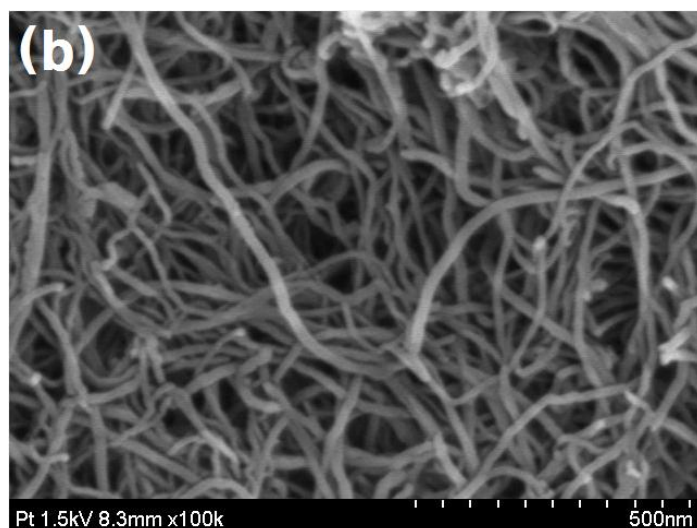
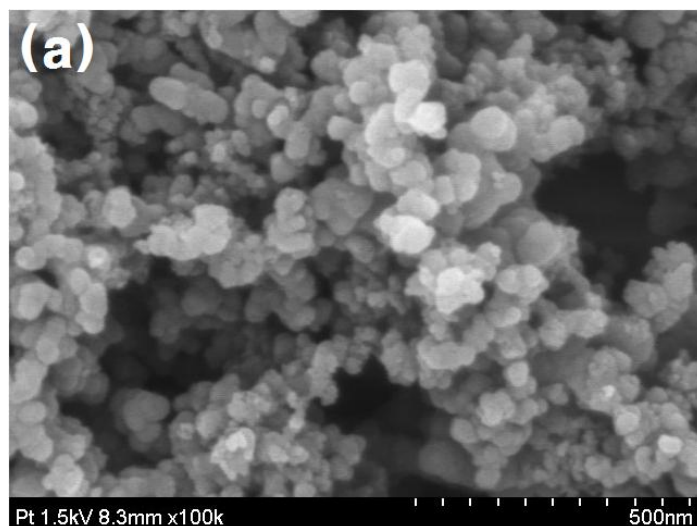


Fig. 7. SEM images of (a) Pt-Ni/VXC, (b) Pt-Ni/CNT, and (c) Pt-Ni/graphene.

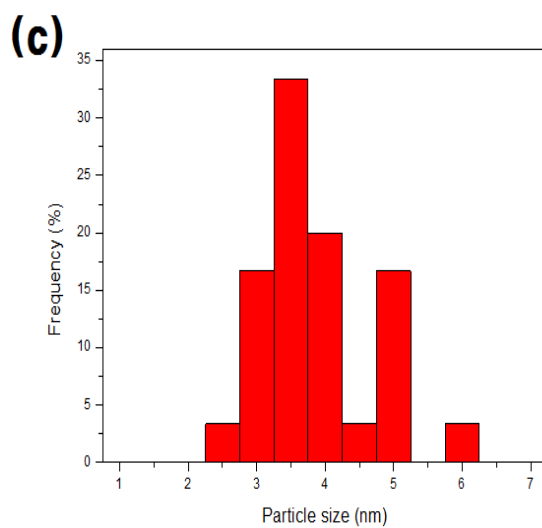
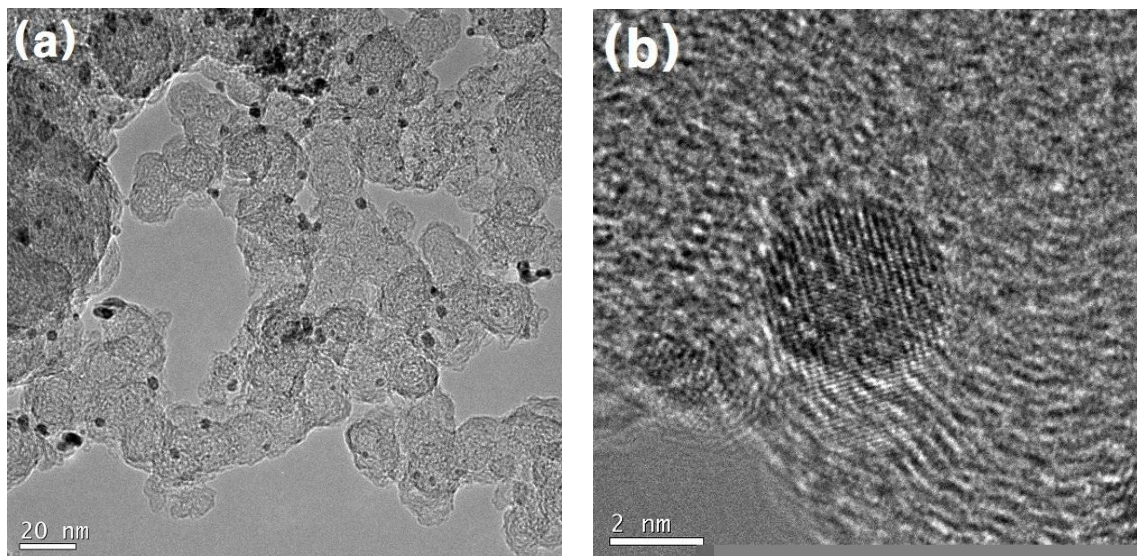


Fig. 8. (a) TEM image, (b) High-resolution TEM image, and (c) Particle size distribution diagram of Pt-Ni/VXC.

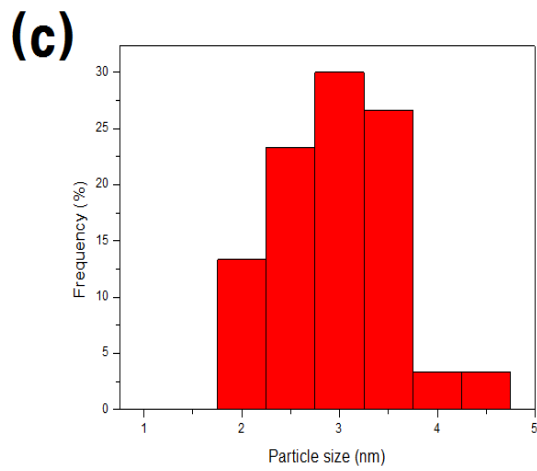
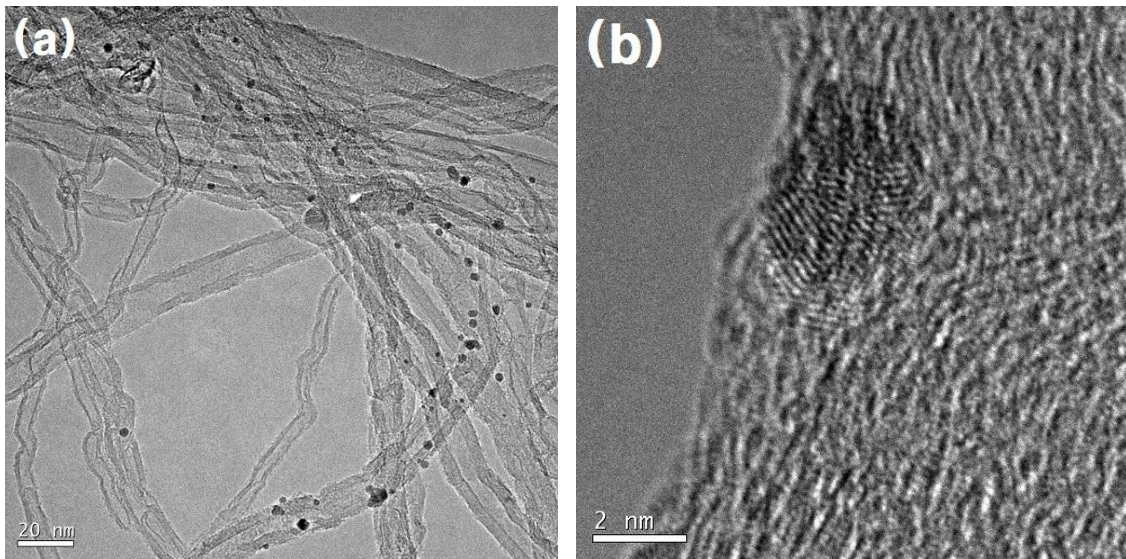


Fig. 9. (a) TEM image, (b) High-resolution TEM image, and (c) Particle size distribution diagram of Pt-Ni/CNT.

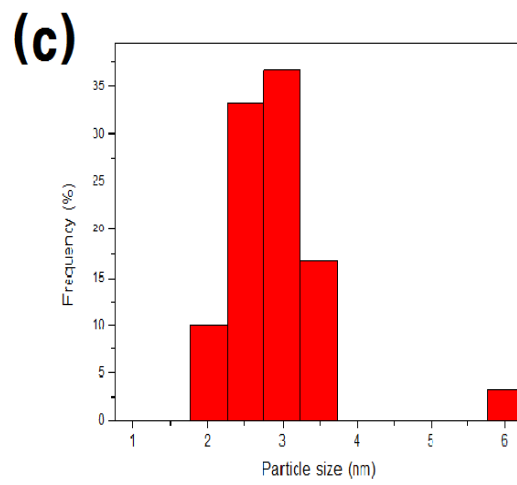
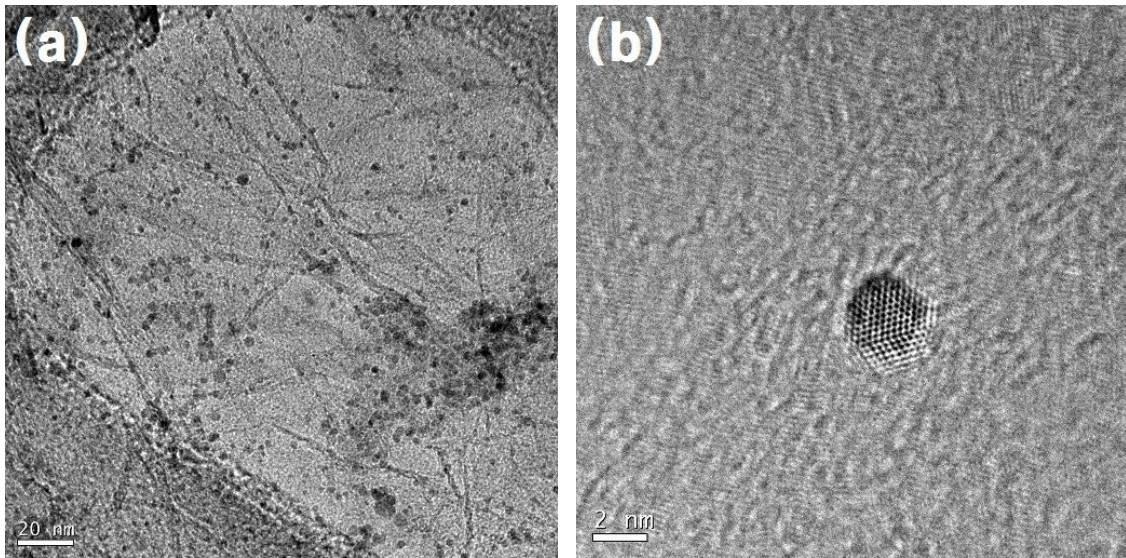


Fig. 10. (a) TEM image, (b) High-resolution TEM image, and (c) Particle size distribution diagram of Pt-Ni/graphene.

### 3.2. Crystalline structure analysis of Pt-Ni based electrocatalysts

The crystal structure and crystallite size of Pt-Ni/VXC, Pt-Ni/CNT, and Pt-Ni/graphene were examined by X-ray diffraction (XRD). As shown in Fig. 11, the XRD patterns of the Pt/graphene, Pt-Ni/VXC, Pt-Ni/CNT, and Pt-Ni/graphene demonstrate the peaks of the Pt fcc structure. However, no characteristic peaks of Ni or Ni oxides are detected in Pt-Ni alloy catalysts.<sup>47</sup> This can be suggested that Pt was alloyed well with Ni. As shown in Fig. 11, the  $2\theta$  of the Pt (1 1 1) peak for Pt-Ni/VXC, Pt-Ni/CNT, and Pt-Ni/graphene are  $41.7^\circ$ ,  $41.7^\circ$ , and  $41.3^\circ$  respectively. Pt peaks of Pt-Ni alloy catalysts was shifted slightly to higher  $2\theta$  angles compared to the pure Pt catalyst. Furthermore, the peaks for Pt-Ni alloy catalysts also became broader. This suggests that interaction between Pt and Ni atoms can be lead to a lattice contraction. Moreover, other small diffraction peaks were also observed around  $33^\circ$  and  $60^\circ$  in Pt-Ni/VXC, Pt-Ni/CNT, and Pt-Ni/graphene. This may be due to the presence of impurities, which increase during high temperature treatment, or substrate of XRD samples. The details of structural characterization are given in Table 3.

The distance between the atomic lattice, D-spacing, was measured using Bragg's law:

$$n\lambda = 2d \sin\theta \quad (1)$$

Where  $n$  is integer ( $n = 1$ ) and  $\lambda$  is the wavelength of the X-ray ( $\lambda = 0.15406$  nm).<sup>48</sup>

Furthermore, XRD patterns of graphite, graphene oxide, and graphene were also evaluated. As shown in Fig. 12, as oxidation proceeds, the intensity of the (0 0 2) diffraction peak decreased dramatically.<sup>50</sup> However, this was observed again when graphene was formed through chemical reduction of graphene oxide. It can be concluded that oxidation of graphite powder was achieved and, ultimately, one layer of graphene nanosheet was formed.

Table 3. Structural characterization of Pt-Ni/VXC, Pt-Ni/CNT, and Pt-Ni/graphene by XRD measurement

Catalysts	Particle size (nm)	D-spacing (nm)	Lattice parameter (nm)
	TEM		
Pt-Ni/VXC	3.45	0.22	0.33
Pt-Ni/CNT	2.73	0.21	0.32
Pt-Ni/graphene	2.67	0.22	0.33

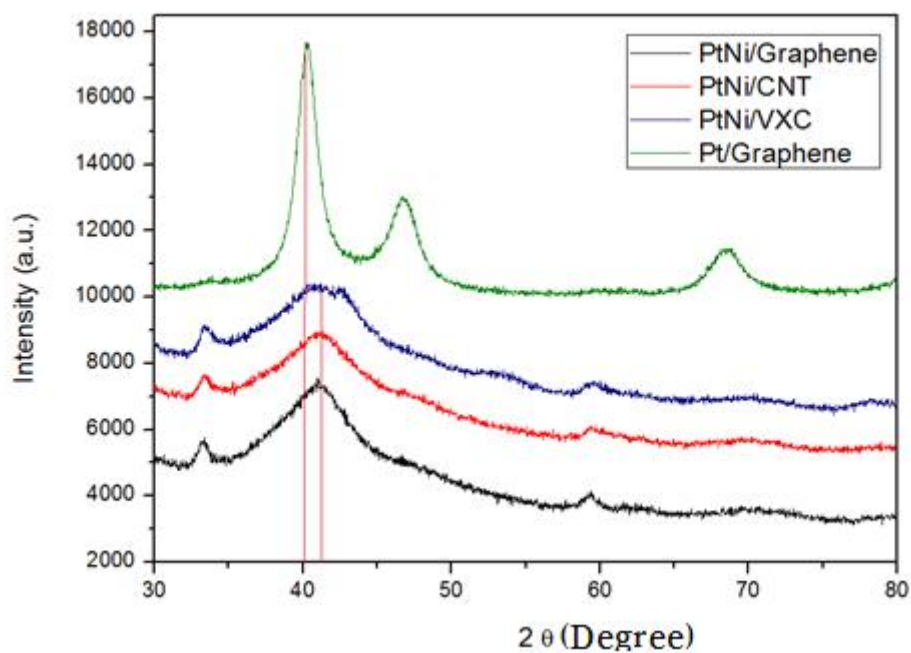


Fig. 11. XRD patterns of the Pt-Ni/VXC, Pt-Ni/CNT, and Pt-Ni/graphene catalysts.

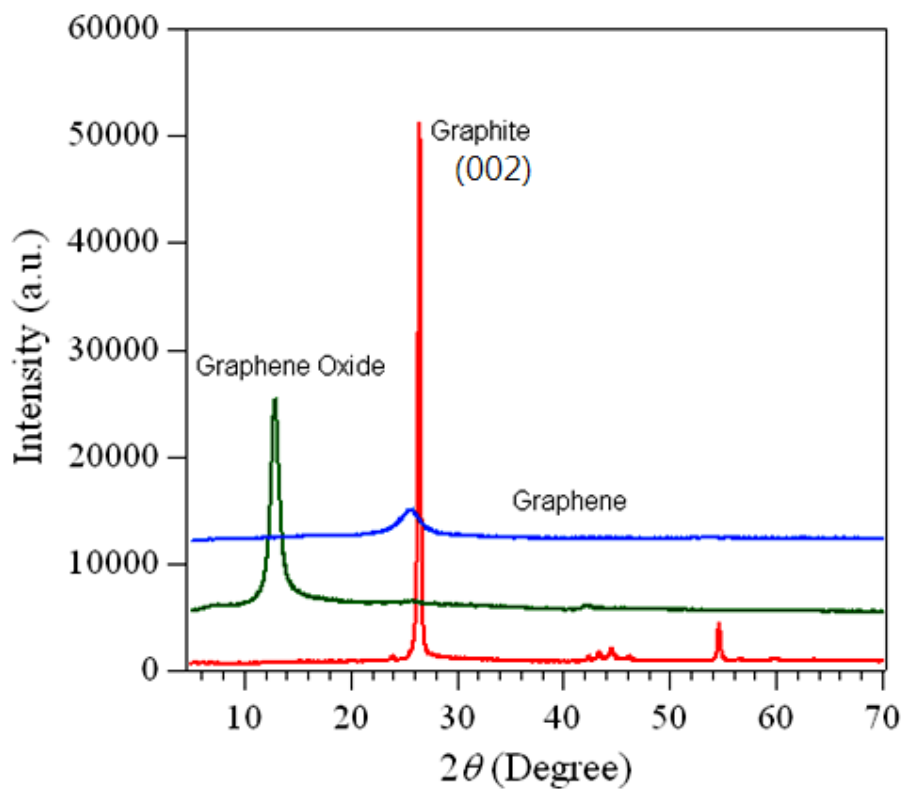


Fig. 12. XRD patterns of graphite, graphene oxide, and graphene.

### 3.3. Chemical and electronic properties of Pt-Ni based electrocatalysts

Electronic structure of Pt-Ni nanoparticles was examined by X-ray photoelectron spectroscopy (XPS). Fig. 13, shows XPS survey spectra of the Pt-Ni alloy supported on three different supports. A main peak with binding energy of around 285 eV is due to the carbon support. Pt and Ni can exist in various oxidized states.<sup>51</sup> Fig. 14 show Pt4f XPS spectrum of Pt-Ni/VXC, Pt-Ni/CNT, and Pt-Ni/graphene. As shown in Fig. 14, Pt in every catalyst was observed as metallic Pt ( $Pt^0$ ), PtO, and PtO<sub>2</sub>. Fig. 14 show Pt4f XPS spectrum of Pt-Ni/VXC, Pt-Ni/CNT, and Pt-Ni/Graphene. As shown in Fig. 14, Pt was observed as  $Pt^0$ , PtO, and PtO<sub>2</sub> for all catalysts. The observed binding energy of  $Pt^0$  for Pt-Ni/VXC (71.29 and 74.49 eV), Pt-Ni/CNT (71.17 and 74.49 eV), and Pt-Ni/graphene (71.17 and 74.39 eV) agrees well with the reported value of  $Pt^0$ .<sup>52,53</sup> The binding energies of PtO and PtO<sub>2</sub> for Pt-Ni/VXC, Pt-Ni/CNT, and Pt-Ni/graphene was also corresponded to the reported values of 72.2 and 74.5 eV respectively (Table 4).<sup>54</sup> Moreover, it was observed that composition of  $Pt^0$  was higher than Pt oxides in all catalysts.

As shown in Fig. 15, metallic Ni ( $Ni^0$ ), Ni oxide (NiO), and Ni hydroxide ( $Ni(OH)_2$ ) exhibits in all catalysts. The binding energy and peak area of the Pt and Ni oxidation states are summarized in Table 4. It has been reported that Ni or Ni hydroxide ( $Ni(OH)_2$ ) are able to oxidize methanol in alkaline or acid solutions, and Pt-Ni alloy catalysts can be protected from corrosion under methanol oxidation.<sup>55</sup> Also, Ni hydroxide has other properties such as proton and electronic conductivity. The presence of Ni oxides such as NiO and  $Ni(OH)_2$  can be lead to increase of the metallic Pt and decrease of Pt oxides states due to the alloy effect of Ni on Pt.<sup>47</sup>

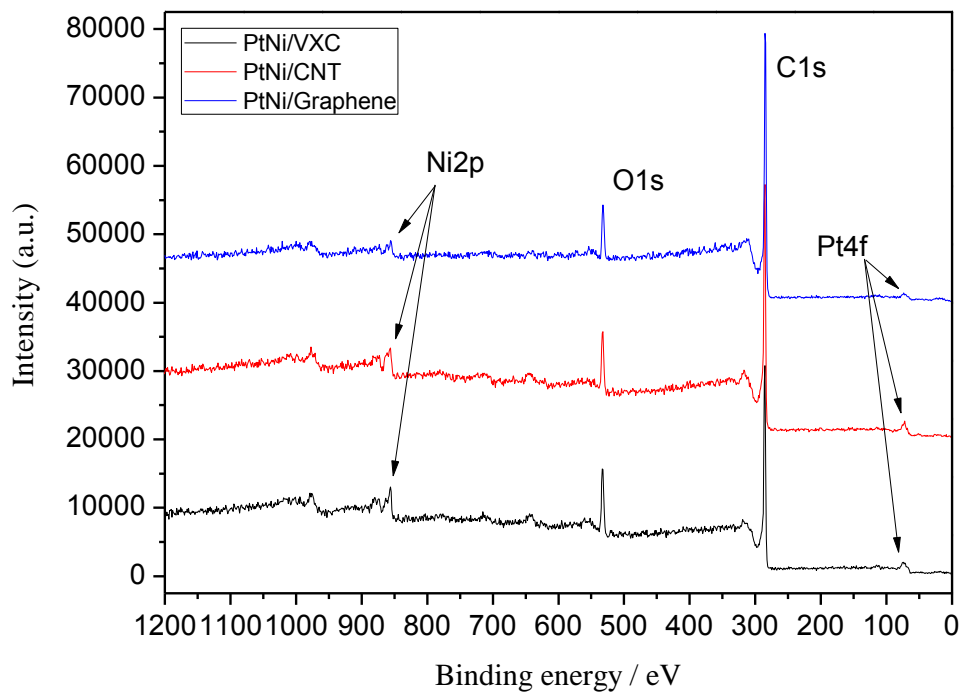


Fig. 13. X-ray photoelectron survey spectra of Pt-Ni/VXC, Pt-Ni/CNT, and Pt-Ni/graphene.

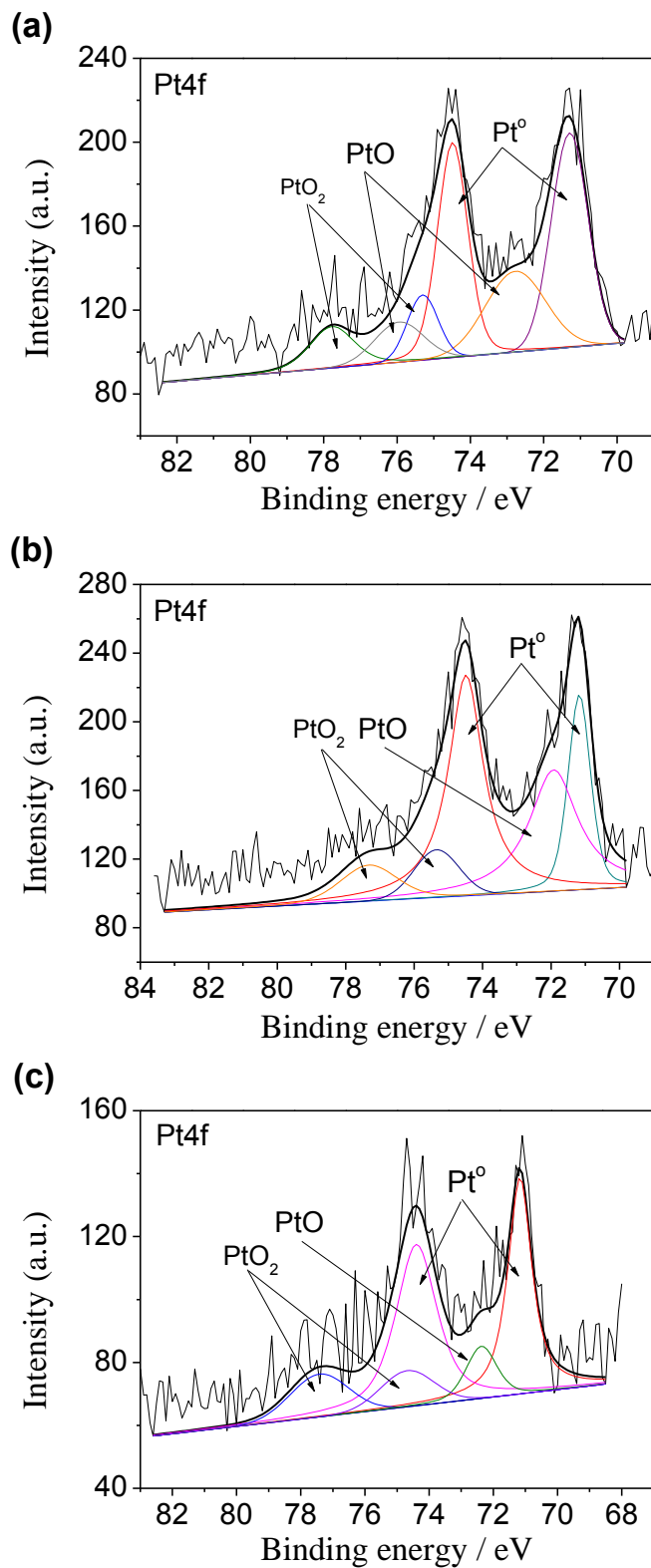


Fig. 14. Pt4f XPS spectra of (a) Pt-Ni/VXC, (b) Pt-Ni/CNT, and (c) Pt-Ni/graphene.

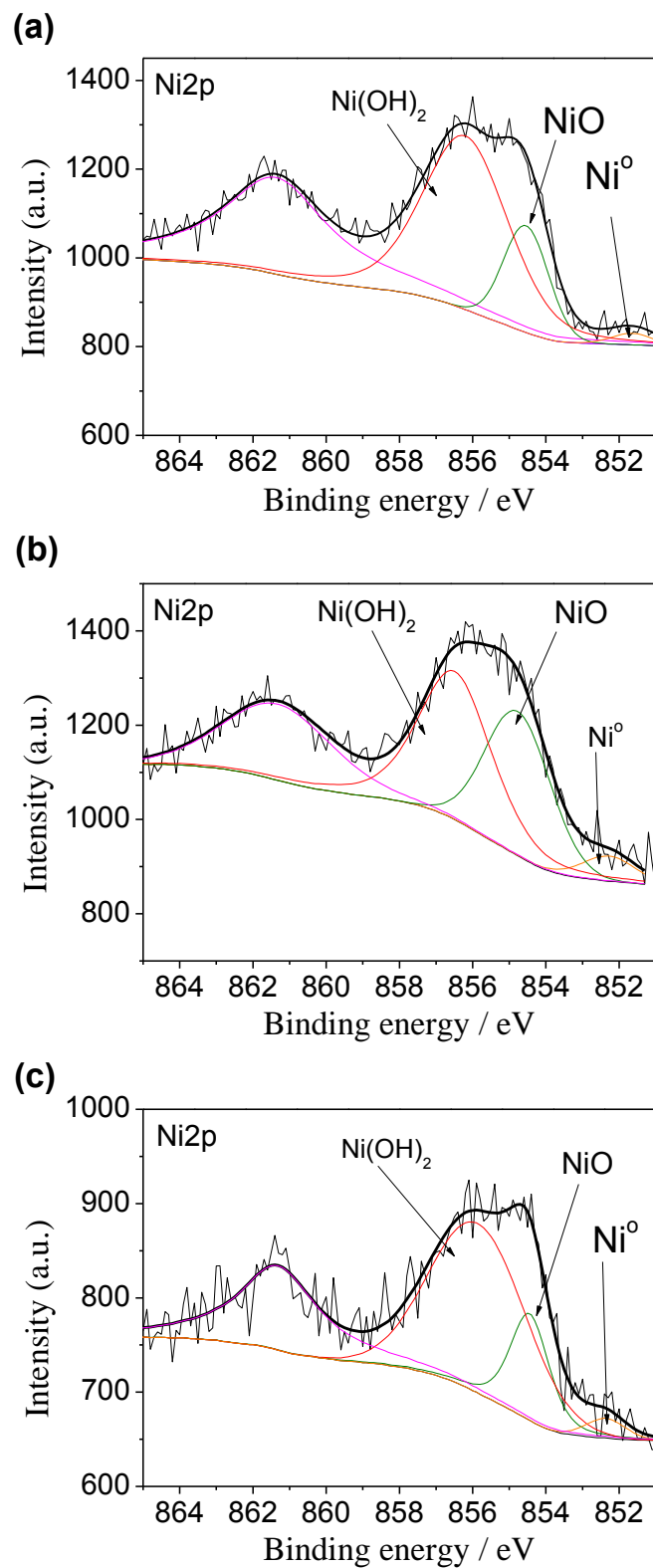


Fig. 15. Ni<sub>2p</sub> XPS spectra of (a) Pt-Ni/VXC, (b) Pt-Ni/CNT, and (c) Pt-Ni/graphene.

Table 4. XPS binding energy (eV) and peak area (%) of possible chemical states of Pt and Ni in the Pt-Ni/VXC, Pt-Ni/CNT, and Pt-Ni/graphene catalysts

Catalysts		Pt			Ni		
		Metallic Pt	PtO	PtO <sub>2</sub>	Metallic Ni	NiO	Ni(OH) <sub>2</sub>
Pt-Ni/VXC	Binding energy (eV)	71.29, 74.49	72.77	75.30, 77.78	851.6	854.5	856.1
	Peak area (%)	63	20	17.3	2.1	21.5	76.3
Pt-Ni/CNT	Binding energy (eV)	71.17, 74.49	71.92	75.34, 77.33	852.3	854.8	856.5
	Peak area (%)	55.8	29.6	14.7	4.4	28.7	39.5
Pt-Ni/graphene	Binding energy (eV)	71.17, 74.39	72.37	74.68, 77.41	852.4	854.4	855.9
	Peak area (%)	71.9	8.4	19.7	2.9	22.5	74

### 3.4. Electrochemical studies of Pt-Ni based electrocatalysts

#### 3.4.1. Electrochemical surface area

Catalytic activity is strongly related to the surface reaction of electrocatalysts. An electrochemically active surface area (ECSA) is an important factor in determining the inherent activities of catalysts.<sup>56</sup> In this section, ESCA measurements and electrocatalytic activities of Pt-Ni alloy catalysts supported on three different carbon materials were studied.

ESCA can be measured from the hydrogen adsorption/desorption region using a cyclic voltammetric (CV) method. As shown in Fig. 16, all catalysts present a hydrogen adsorption region from 0.3 to 0.07 V of potential range after cathodic sweep, while the hydrogen desorption region was presented from 0.06 to 0.36 V of potential range after anodic sweep. ESCA can be calculated from these two charge areas ( $Q_{H_2 \cdot \text{adsorption}}$  and  $Q_{H_2 \cdot \text{desorption}}$ ) and the amount of Pt loading on the electrode:<sup>57</sup>

$$\text{ECSA} = \frac{Q_H}{[\text{Pt}] \times 0.21}$$

Where,  $Q_H$  is the charge for hydrogen desorption (mC). [Pt] represents the platinum loading ( $\text{mg cm}^{-2}$ ) in the electrode and the value of 0.21 is known as the charge for the monolayer of hydrogen adsorption on the Pt surface.<sup>58</sup>

The values of  $Q_H$  and ECSA of Pt-Ni/VXC, Pt-Ni/CNT, and Pt-Ni/graphene catalysts were listed in table 6. It was found that all three catalysts show a similar active surface area (around  $30 \text{ m}^2 \text{ g}^{-1}$ ). However, Pt-Ni/graphene catalyst showed a higher ECSA among the three catalysts.

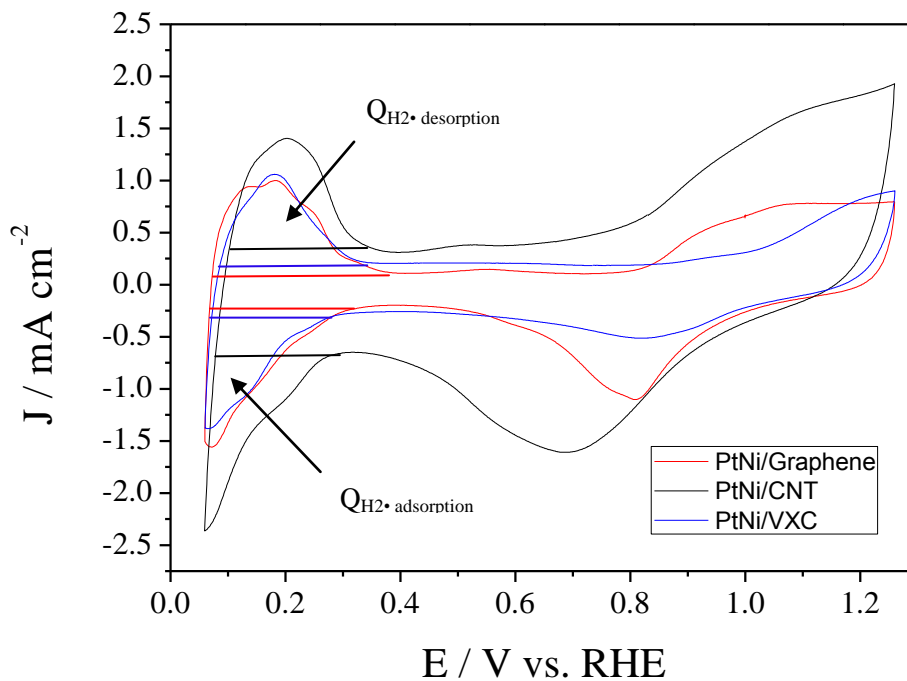


Fig. 16. Cyclic voltammogram of Pt-Ni/VXC, Pt-Ni/CNT, and Pt-Ni/graphene catalysts in  $N_2$ -saturated  $0.5\text{ M H}_2\text{SO}_4$  with a scan rate of  $20\text{ mVs}^{-1}$  at  $25^\circ\text{C}$ .

Table 5. The value of  $Q_H$  and ECSA, of Pt-Ni/VXC, Pt-Ni/CNT, and Pt-Ni/graphene catalysts

Catalysts	$Q_H$ (mC)	ECSA ( $\text{m}^2\text{ g}^{-1}$ )
Pt-Ni / VXC	$7.0 \pm 0.05$	$31.1 \pm 0.05$
Pt-Ni / CNT	$6.5 \pm 0.05$	$30.1 \pm 0.05$
Pt-Ni / graphene	<b><math>8.6 \pm 0.05</math></b>	<b><math>32.0 \pm 0.05</math></b>

### 3.4.2. Oxygen reduction reaction activities of Pt-Ni based electrocatalysts

ORR activities of Pt-Ni/VXC, Pt-Ni/CNT, and Pt-Ni/graphene catalysts were measured by rotating disk electrode (RDE) in a 0.5 M H<sub>2</sub>SO<sub>4</sub> electrolyte. For the comparison, Pt/C (20 wt%) was also used. The RDE traces and Koutechy-Levich plot of Pt-Ni/VXC, Pt-Ni/CNT, and Pt-Ni/graphene is illustrated in Fig. 17. In Fig. 18, it can be identified that all catalysts showed charge transfer from the onset potential region (0.85 to 0.98 V vs. RHE). Furthermore, the ORR for all of the samples revealed mixed diffusion-kinetic control in the potential region from 0.65 to 0.85 V. Moreover, the limiting current density for the samples showed a plateau behavior in the potential region between 0.26 V to 0.65 V. This means that the ORR of all samples was diffusion controlled under the potential region of 0.26 V to 0.65 V. This limiting current density can be both increased and decreased by virtue of the rotating rate<sup>59</sup>. the limiting current density can be controlled by the mass transport rate.<sup>60</sup>

To compare the ORR activities of all samples, 1600 rpm of rotating rate was selected. As shown in Fig. 18, the onset potential was decreased in order of Pt-Ni/graphene (0.98V), Pt-Ni/VXC (0.93 V), Pt-Ni/CNT (0.89 V), and Pt/C (0.85 V) at the rotation speed of 1600 rpm. Moreover, Pt-Ni/graphene showed the highest half wave potential among three catalysts (0.77 V). Half wave potentials, defined as the potential at the measured current reaches the half of the limiting current.<sup>61</sup> ORR activities of all Pt-Ni alloy catalysts supported on VXC, CNT, and graphene registered higher ORR activities than the commercial Pt/C catalyst. In addition, the Pt-Ni/graphene catalyst had the highest ORR activity catalyst among four samples. The K-L plots of all samples, illustrated in Fig. 17, is derived from the Koutechy-Levich equation:<sup>62,63</sup>

$$\frac{1}{j} = \frac{1}{j_k} + \frac{1}{B\omega^{1/2}}$$

$$B = 0.62 nFC_b D_o^{2/3} \nu^{-1/6}$$

Where,  $n$  is the number of electrons transferred in the ORR,  $F$  is the Faraday constant ( $96,485 \text{ C mol}^{-1}$ ),  $C_b$  is the bulk concentration of  $\text{O}_2$  ( $1.1 \times 10^{-3} \text{ mol cm}^{-3}$ ),  $D_o$  is the diffusion coefficient of  $\text{O}_2$  ( $1.93 \times 10^{-5} \text{ cm}^2 \text{ s}^{-1}$ ), and  $\nu$  is the viscosity of the electrolyte. In the case of  $0.5 \text{ M H}_2\text{SO}_4$ ,  $\nu$  has been reported as  $0.01 \text{ cm}^2 \text{ s}^{-1}$ .  $\omega$  indicates the angular rotation rate of the electrode. Kinetic current density ( $j_k$ ) was obtained from various voltages from the ORR curve ( $0.3\text{V}$  to  $0.6\text{V}$  vs. RHE), and it was plotted as a function of  $\omega^{-1/2}$ . K-L plots show linearity, and it can be concluded that the ORR for all samples was followed a first order of kinetic (Fig. 17).

Furthermore, as shown in Fig. 18, both mass activities and specific activities of Pt-Ni/VXC, Pt-Ni/CNT, and Pt-Ni/graphene catalysts were evaluated with ECSA data and an RDE curve at  $0.8 \text{ V}$  in a  $0.5 \text{ M H}_2\text{SO}_4$  electrolyte. Pt-Ni/graphene was shown the highest activity and, according to oxygen reduction current density, both mass activities and specific activities, of all catalysts follows the order of Pt-Ni/graphene > Pt-Ni/VXC > Pt-Ni/CNT.

The rotating ring-disc electrode (RRDE) method was also used to measure the production of hydrogen peroxide ( $\text{H}_2\text{O}_2$ ) which is generated during ORR. The ORR occurs at the disk electrode and generated  $\text{H}_2\text{O}_2$  is either oxidized or reduced on the ring electrode where located around disk electrode.<sup>46</sup> Fig. 20 illustrates (a)  $\text{H}_2\text{O}_2$  oxidation curve on the ring electrode and (b) oxygen reduction curves on the disk electrode. As shown in Fig. 20, ORR activities on the disk electrode were measured as similar to those using the RDE technique. The ORR activity was increased in the order of Pt-Ni/graphene > Pt-Ni/VXC > Pt-Ni/CNT. The number of electron transfer was followed near four. This suggests that small amounts of  $\text{H}_2\text{O}_2$ , less than 3%, was detected on the ring electrode for all three Pt-Ni based catalysts. Detail values are listed in Table 7. The  $\text{H}_2\text{O}_2$  formation was minimum on Pt-Ni/graphene among the investigated three catalysts.

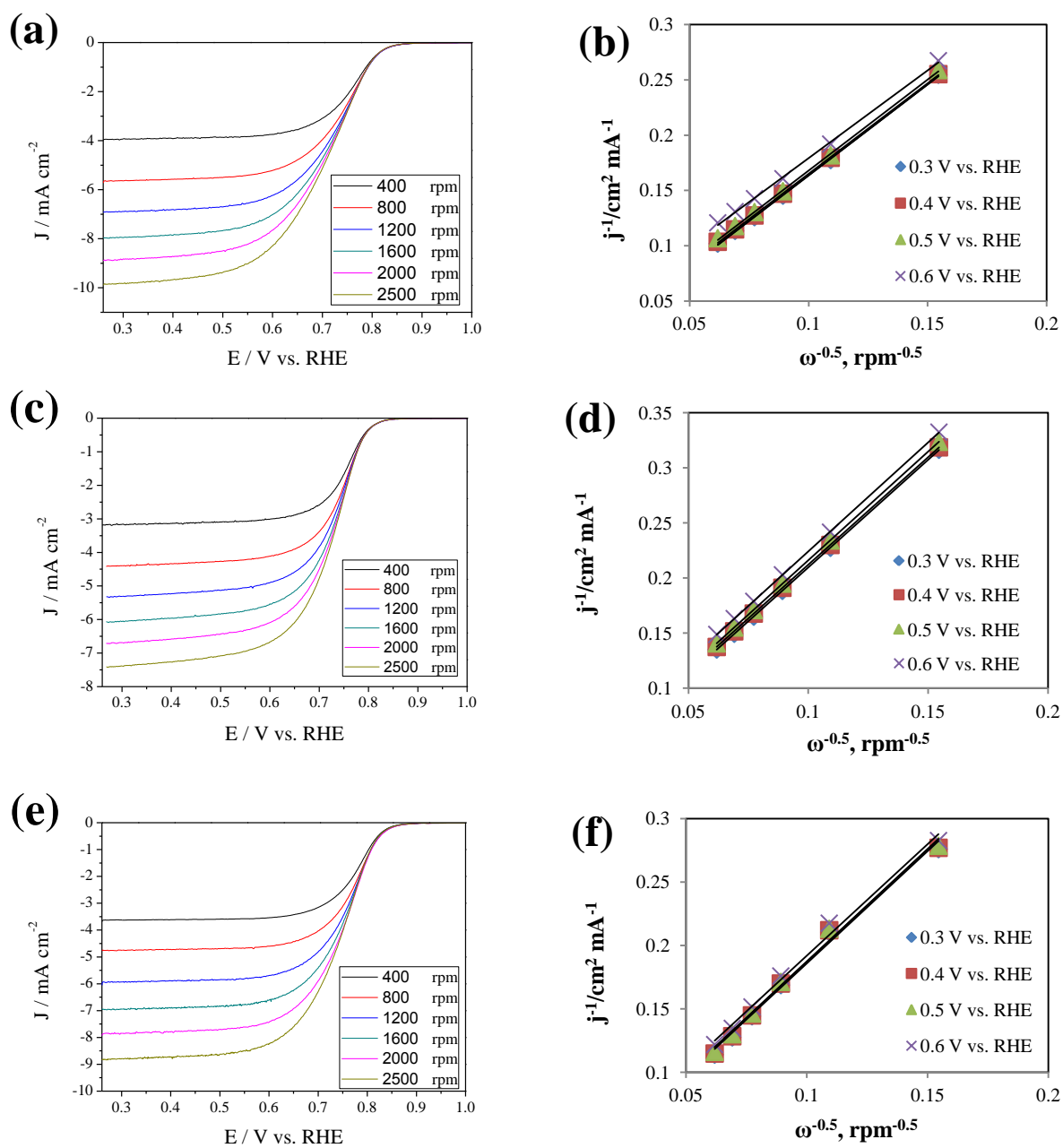


Fig. 17. RDE traces of (a) Pt-Ni/VXC, (c) Pt-Ni/CNT, and (e) Pt-Ni/graphene and Koutechy-Levich plot of (b) Pt-Ni/VXC, (d) Pt-Ni/CNT, and (f) Pt-Ni/graphene catalysts in  $O_2$ -saturated 0.5 M  $H_2SO_4$  with a scan rate of  $5 \text{ mVs}^{-1}$  at room temp.

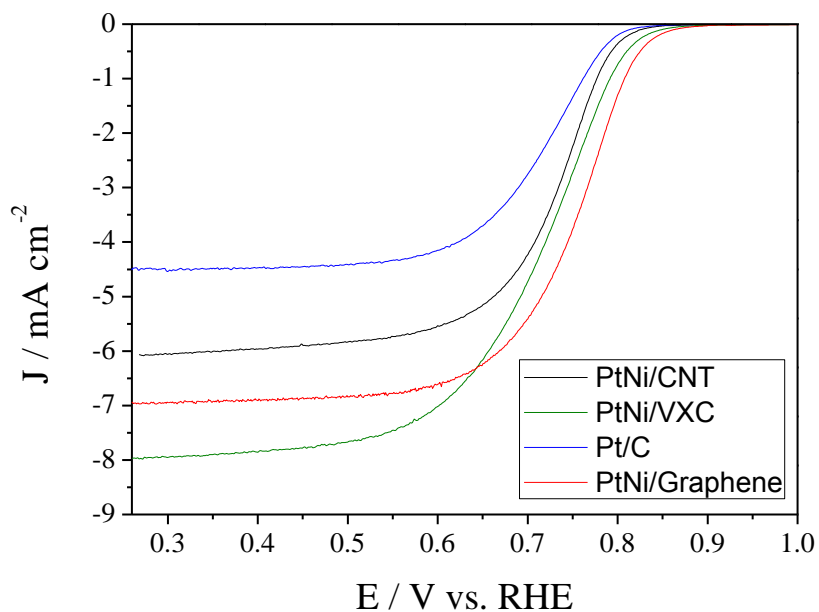


Fig. 18. Comparison of ORR activities of Pt/C, Pt-Ni/VXC, Pt-Ni/CNT, and Pt-Ni/graphene catalysts in  $\text{O}_2$ -saturated 0.5 M  $\text{H}_2\text{SO}_4$  with a scan rate of  $5 \text{ mVs}^{-1}$  at room temp; rotating speed: 1600 rpm.

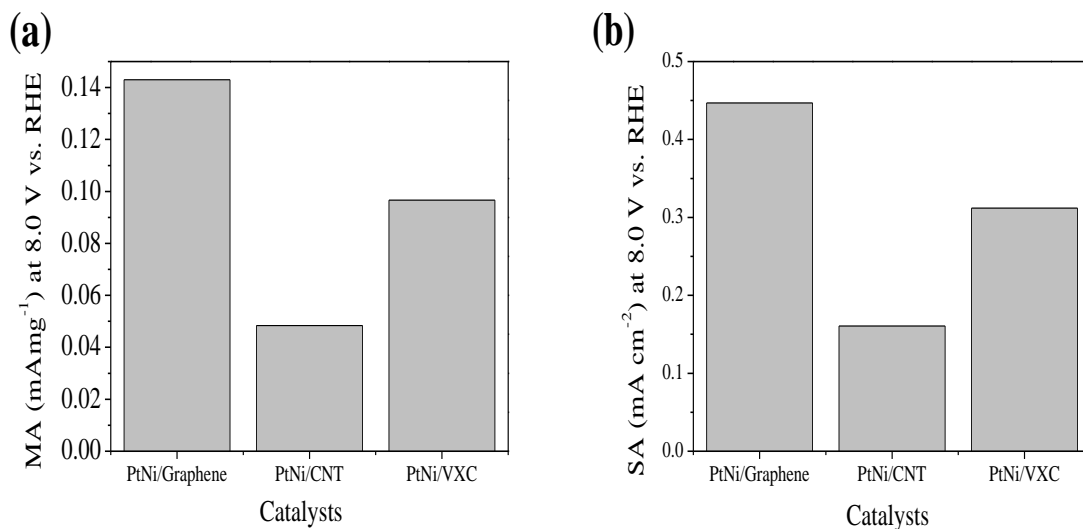


Fig. 19. (a) Mass and (b) Specific activities of Pt-Ni/VXC, Pt-Ni/CNT, and Pt-Ni/graphene catalysts at 0.8 V in a 0.5 M  $\text{H}_2\text{SO}_4$  electrolyte.

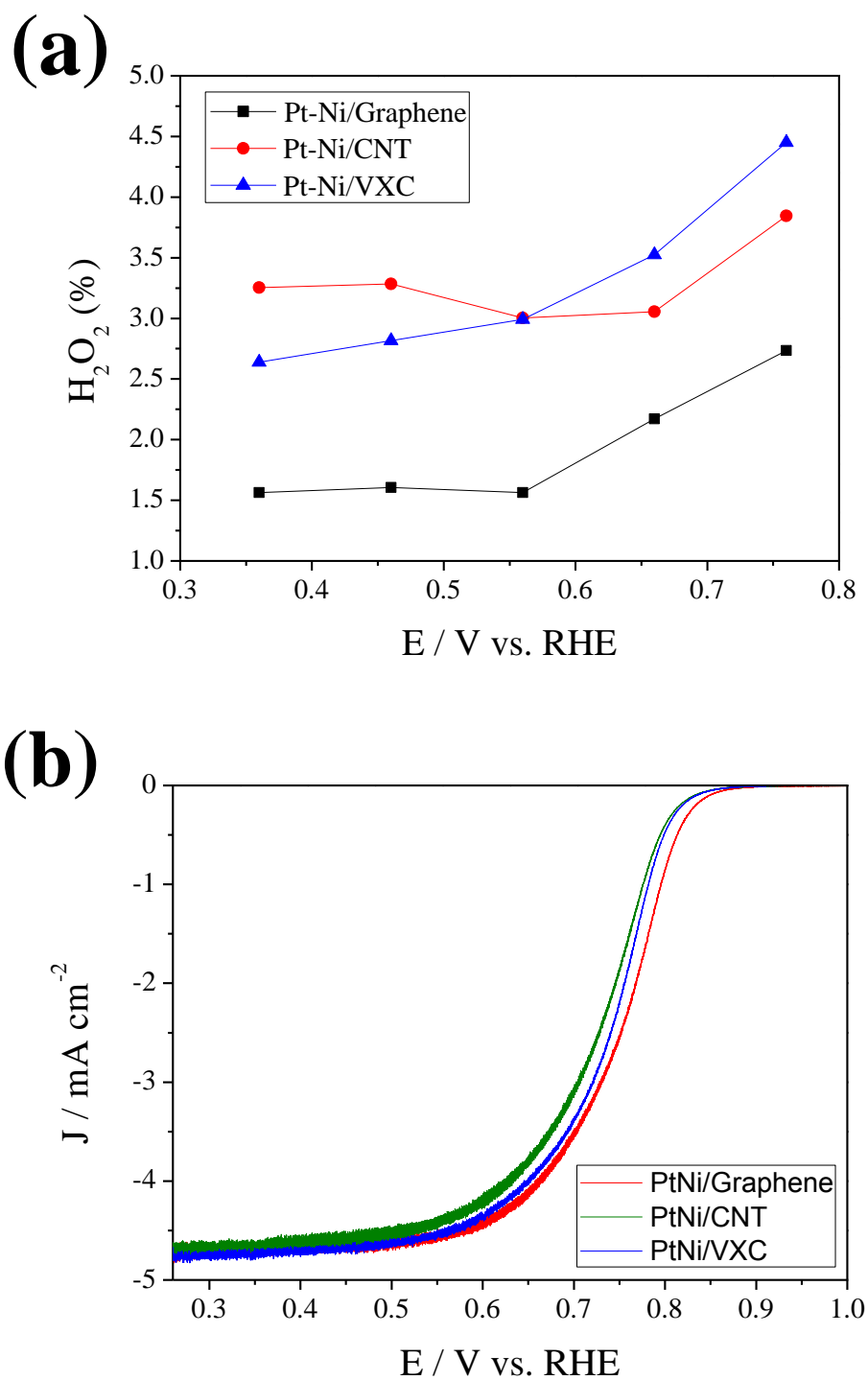


Fig. 20 (a) Percentage of  $\text{H}_2\text{O}_2$  formation on the ring and (b) Oxygen reduction curves of Pt-Ni/VXC, Pt-Ni/CNT, and Pt-Ni/graphene catalysts measured by RRDE in  $\text{O}_2$ -saturated 0.5 M  $\text{H}_2\text{SO}_4$  with a scan rate of  $5 \text{ mVs}^{-1}$  at room temp; rotating speed: 1600 rpm.

Table 6. Electrochemical analysis of Pt-Ni/VXC, Pt-Ni/CNT, and Pt-Ni/graphene catalysts

Catalysts	Mass activities (mA mg <sup>-1</sup> )	Specific activities (mA cm <sup>-2</sup> )	Number of electrons transferred (n)	H <sub>2</sub> O <sub>2</sub> production (%) at 0.75 V vs. RHE
Pt-Ni/VXC	0.097	0.31	3.91	4.45
Pt-Ni/CNT	0.048	0.16	3.92	3.84
Pt-Ni/graphene	0.14	0.45	3.95	2.73

### 3.4.3. Methanol tolerance studies of Pt-Ni based electrocatalysts

It is known that methanol crossover decreases the efficiency of direct methanol fuel cell (DMFC) systems.<sup>64</sup> This is because Pt/C is generally used as the catalyst on the cathodic site, and methanol from the anode would be oxidized at the cathode.<sup>65</sup> To avoid these unfavorable methanol effects on the cathode in DMFCs, numerous experiments have been carried out. In this work, Pt-Ni alloy catalysts supported on VXC, CNT, and graphene were evaluated for methanol tolerance in acidic media.

Figs. 21 and 22 show the ORR activities in the presence of 0.5 M CH<sub>3</sub>OH. In the presence of methanol, an ORR activity of all Pt-Ni alloy catalysts was decreased. However, potential loss of all three catalysts was noticeably low. Measured potential loss was as about only 20 mV, 23 mV, and 34 mV for Pt-Ni/graphene, Pt-Ni/CNT, and Pt-Ni/VXC, respectively. In addition, the current density at 0.8 V is decreased in order of Pt-Ni/graphene > Pt-Ni/CNT > Pt-Ni/VXC. It can be concluded that Pt-Ni alloy catalysts showed strong methanol tolerance during the ORR.<sup>66</sup> Moreover, Pt-Ni/graphene indicated the highest methanol tolerance among the three catalysts.

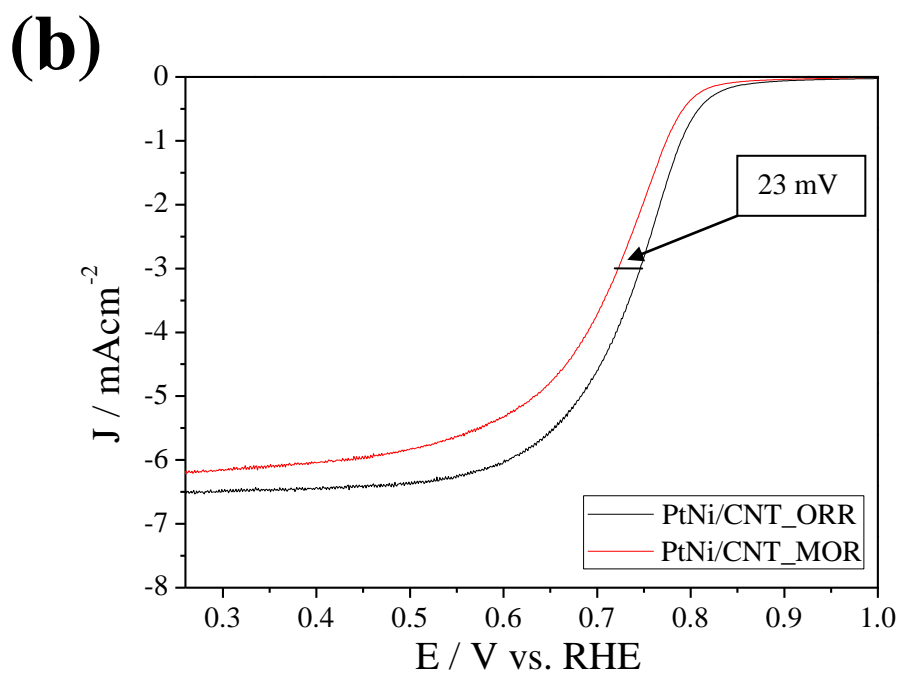
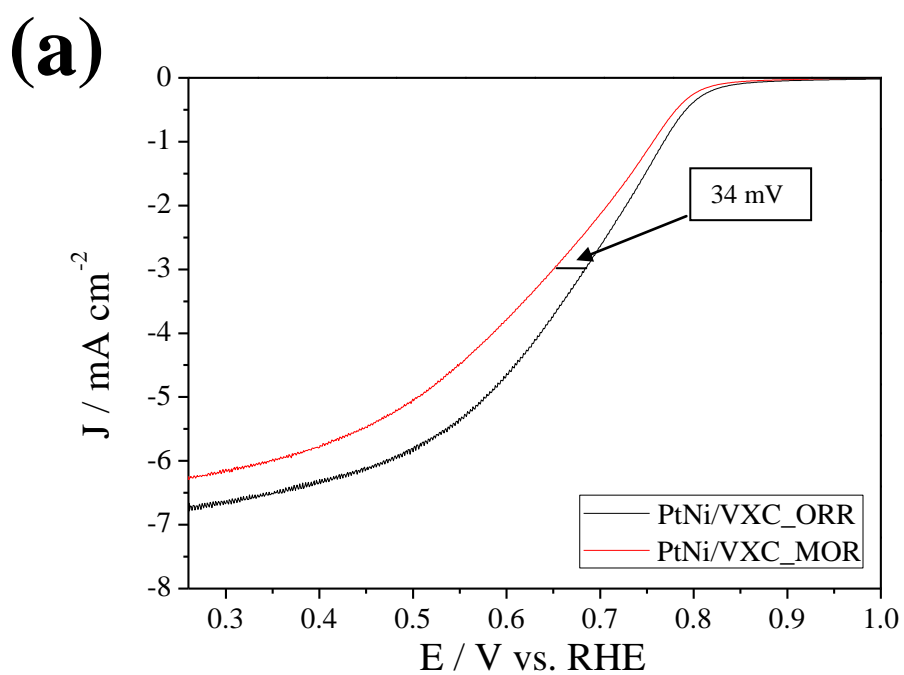


Fig. 21. Liner sweep voltammograms of (a) Pt-Ni/VXC and (b) Pt-Ni/CNT in an  $\text{O}_2$ -saturated 0.5 M  $\text{H}_2\text{SO}_4$  + 0.5 M  $\text{CH}_3\text{OH}$  electrolyte with a scan rate of  $5 \text{ mV s}^{-1}$  at room temp; rotating speed: 1600 rpm.

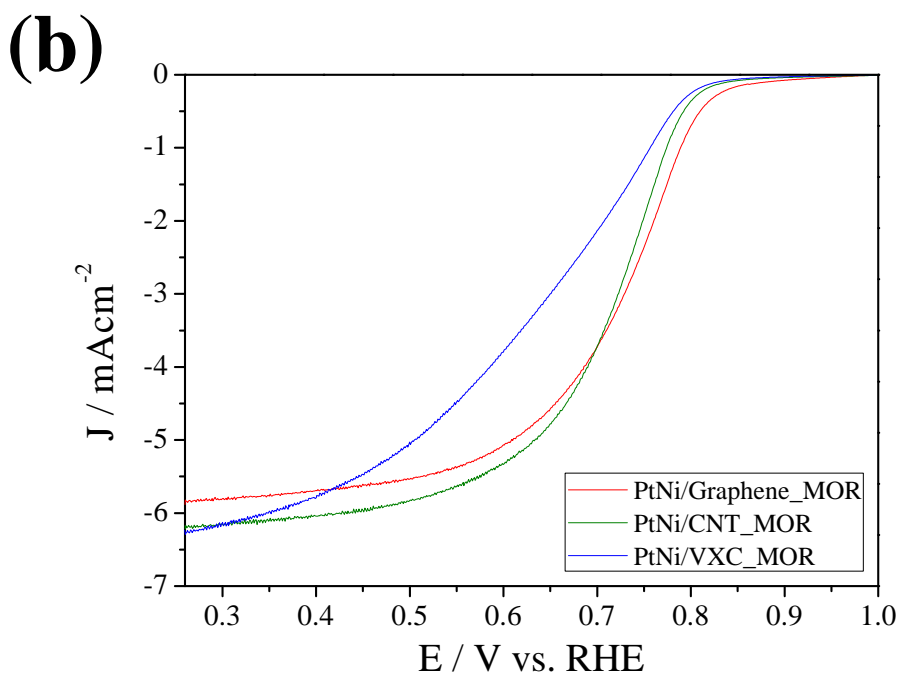
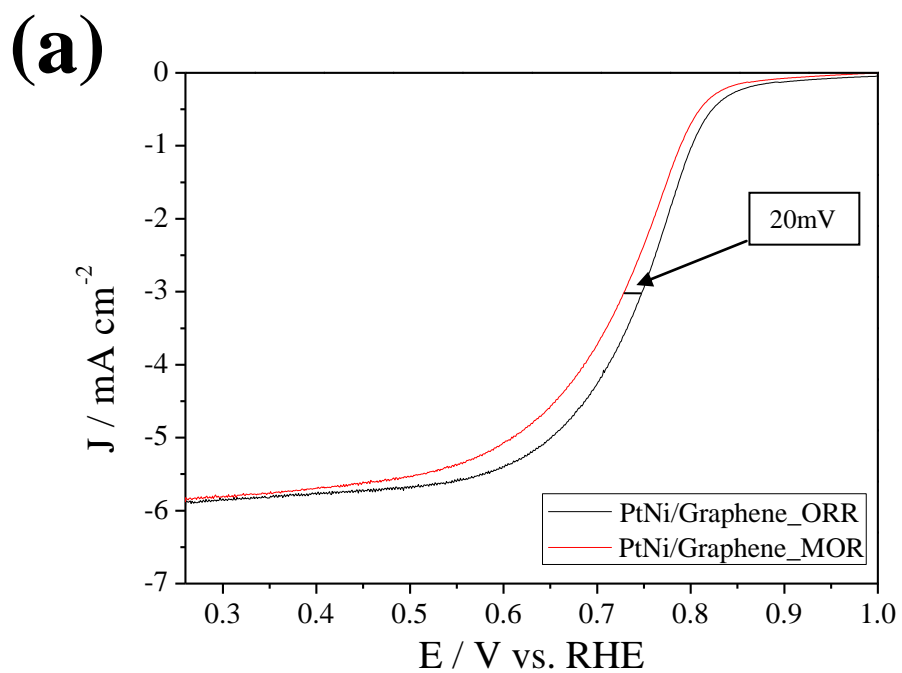


Fig. 22. Linear sweep voltammograms of (a) Pt-Ni/graphene and (b) Pt-Ni alloy catalysts in an  $\text{O}_2$ -saturated  $0.5 \text{ M H}_2\text{SO}_4 + 0.5 \text{ M CH}_3\text{OH}$  electrolyte with a scan rate of  $5 \text{ mV s}^{-1}$  at room temp; rotating speed: 1600 rpm.

### 3.4.4. Stability of Pt-Ni based electrocatalysts

It is known that the cathode of the fuel cells is operated under an acidic environment, and this causes corrosion of metal catalysts. Since corrosion is directly related to fuel cell performance, the stability of the catalysts should be studied.<sup>67</sup>

In this section, an accelerated stability test (AST) of Pt-Ni based electrocatalysts was studied. AST was performed by using CV measurement. The ECSA was evaluated from 20 to 2000 cycles in an N<sub>2</sub> saturated 0.5 M H<sub>2</sub>SO<sub>4</sub> electrolyte. As shown in Fig. 23, after 2000 cycles, only 3.4 % of the initial ECSA of Pt-Ni/graphene remained. On the other hand, the ECSA of Pt-Ni/VXC and Pt-Ni/CNT showed better results, as 23.4 and 20 % remained, respectively. The ECSA of all samples decreased sharply between 20 to 500 cycles. The decrease in ECSA values is listed in Table 8. Contrary to ORR activities, in the AST Pt-Ni/Graphene shows the lowest stability under acidic media.

The degradation of ECSA can be caused by the dissolution and agglomeration of the Pt based nanoparticles.<sup>68</sup> In other word, long term exposure of Pt based nanoparticles in acidic media can cause agglomerations of metal nanoparticles, and it leads to low stability. However, it can be improved by using non-noble electrocatalysts. Non-noble catalyst materials, such as nitrogen doped carbon support materials, were also reported to improve electrochemical stabilities of Pt based catalysts in acid solutions.<sup>69</sup>

Table 7. ECSA decrement of Pt-Ni/VXC, Pt-Ni/CNT, and Pt-Ni/Graphene catalysts by CV

Catalysts	The decrease of ECSA (%)
Pt-Ni/VXC	76.6
Pt-Ni/CNT	80.0
Pt-Ni/graphene	96.6

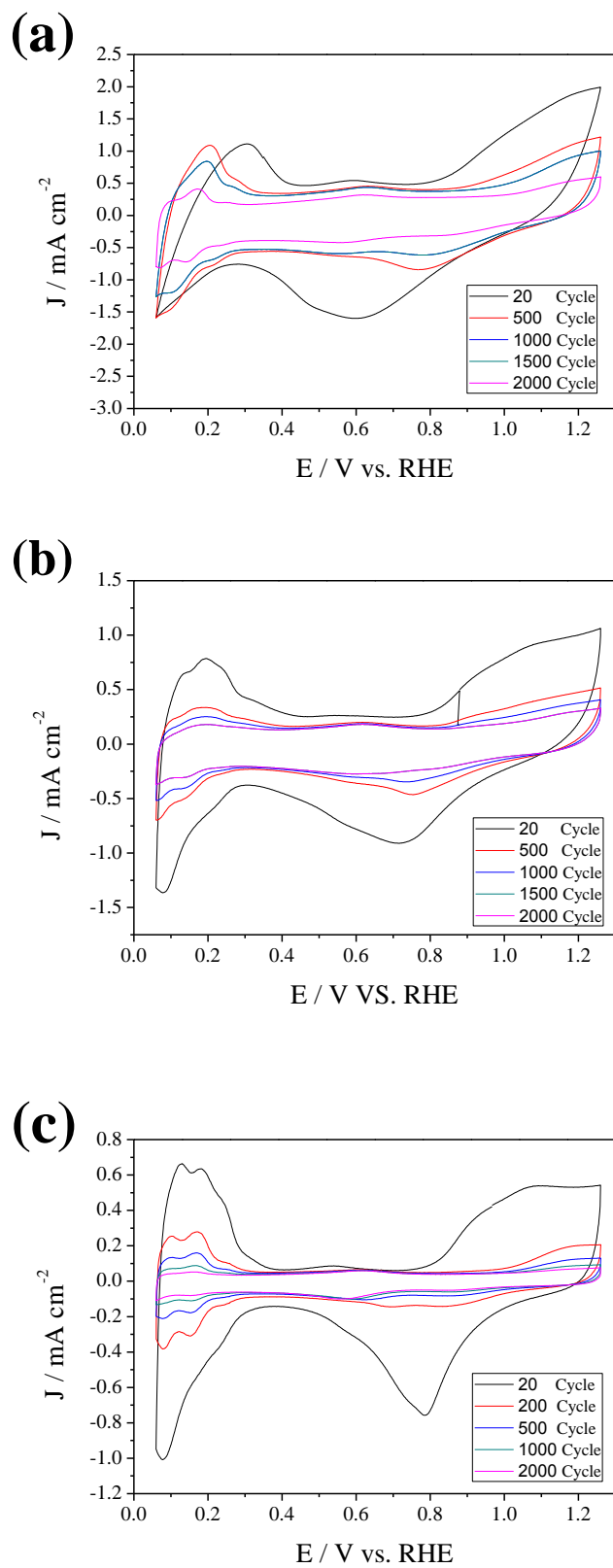


Fig. 23. Accelerated stability test of (a) Pt-Ni/VXC, (b) Pt-Ni/CNT, and (c) Pt-Ni/graphene by CV in  $N_2$ -saturated 0.5 M  $H_2SO_4$  with a scan rate of  $50 \text{ mV s}^{-1}$  at room temp.

## Conclusions

The oxygen reduction reaction (ORR) on the cathode is responsible for a large part of fuel cell performance. Enormous research studies have been carried out to improve ORR activities in the fuel cell systems. In addition, a high dependence on platinum catalysts has blocked the commercialization and applications of fuel cells.

To increase ORR activities and decrease amount of platinum catalysts, Pt-Ni alloy electrocatalysts supported on various carbon materials such as carbon black (Vulcan carbon XC-72, VXC), carbon nanotube, and graphene were investigated as cathode catalyst for a Polymer electrolyte membrane fuel cells (PEMFCs). Novel carbon materials such as graphene have garnered attention as alternative material for carbon support due to their favorable properties.

It was observed by TEM studies that 20 wt. % of Pt-Ni (1:1) alloy catalysts had particle size of less than 5 nm. Moreover, nanoparticles were dispersed uniformly on carbon support materials. This suggests that there was no agglomeration of nanoparticles. The physical structure of Pt-Ni alloy catalysts and graphene was analyzed by XRD measurement. Pt (1 1 1) diffraction peaks was shifted slightly to a positive direction. It can be concluded that Ni was well alloyed with Pt in all samples, and the presence of Ni can be caused electronic structure changes of Pt nanoparticles.

Moreover, both metallic and oxide forms of Pt and Ni nanoparticles were investigated by XPS. It was found that amount of metallic Pt was more than 50 % compared to Pt oxide states such as PtO and PtOH. Also, Ni exhibited as a Ni oxide state more than as a metallic state. This can result in an increase of the metallic Pt and a decrease of the Pt oxide state because of electronic interaction between Pt and Ni.

Electrochemical studies of Pt-Ni based electrocatalysts were also carried out to identify ORR activities. Among three catalysts, Pt-Ni/graphene showed the highest ORR activities, and all Pt-Ni alloy catalysts were followed the direct 4 electron pathway. Also, Pt-Ni/graphene catalysts showed highest methanol resistance. However, it showed the lowest performance in the accelerated stability test (AST). It can be concluded that dissolution and agglomeration occurred when the Pt based

nanoparticles were exposed to an acidic environment. Improvement of the stability and durability of noble metal catalysts for fuel cells should be considered for the future studies.

## Reference

- 1 Gottesfeld, S. & Zawodzinski, T. A. in *Advances in Electrochemical Science and Engineering* 195-301 (Wiley-VCH Verlag GmbH, 2008).
- 2 Yonghong Bing , H. L., Lei Zhang , Dave Ghosh and Jiujun Zhang Nanostructured Pt-alloy electrocatalysts for PEM fuel cell oxygen reduction reaction. *Chem. Soc. Rev* **39**, 2184-2202, doi:10.1039/B912552C (2009).
- 3 Maass, S., Finsterwalder, F., Frank, G., Hartmann, R. & Merten, C. Carbon support oxidation in PEM fuel cell cathodes. *Journal of Power Sources* **176**, 444-451, doi:http://dx.doi.org/10.1016/j.jpowsour.2007.08.053 (2008).
- 4 Antolini, E. Carbon supports for low-temperature fuel cell catalysts. *Applied Catalysis B: Environmental* **88**, 1-24, doi:http://dx.doi.org/10.1016/j.apcatb.2008.09.030 (2009).
- 5 Iijima, S. Carbon nanotubes: past, present, and future. *Physica B: Condensed Matter* **323**, 1-5, doi:http://dx.doi.org/10.1016/S0921-4526(02)00869-4 (2002).
- 6 Geim, A. K. & Novoselov, K. S. The rise of graphene. *Nat Mater* **6**, 183-191 doi:10.1038/nmat1849 (2007).
- 7 Schmidt, T. J., Paulus, U. A., Gasteiger, H. A. & Behm, R. J. The oxygen reduction reaction on a Pt/carbon fuel cell catalyst in the presence of chloride anions. *Journal of Electroanalytical Chemistry* **508**, 41-47, doi:10.1016/s0022-0728(01)00499-5 (2001).
- 8 Toda, T., Igarashi, H. & Watanabe, M. Role of Electronic Property of Pt and Pt Alloys on Electrocatalytic Reduction of Oxygen. *Journal of The Electrochemical Society* **145**, 4185-4188, doi:10.1149/1.1838934 (1998).
- 9 Li, W., Xin, Q. & Yan, Y. Nanostructured Pt–Fe/C cathode catalysts for direct methanol fuel cell: The effect of catalyst composition. *International Journal of Hydrogen Energy* **35**, 2530-2538, doi:10.1016/j.ijhydene.2010.01.013 (2010).
- 10 Xiong, L., Kannan, A. M. & Manthiram, A. Pt–M (M=Fe, Co, Ni and Cu) electrocatalysts synthesized by an aqueous route for proton exchange membrane fuel cells. *Electrochemistry*

- Communications* **4**, 898-903, doi:10.1016/s1388-2481(02)00485-x (2002).
- 11 Acres, G. J. K. Recent advances in fuel cell technology and its applications. *Journal of Power Sources* **100**, 60-66, doi:10.1016/s0378-7753(01)00883-7 (2001).
  - 12 Larminie, J. & Dicks, A. (John Wiley & Sons).
  - 13 Schäfer, A., Heywood, J. B. & Weiss, M. A. Future fuel cell and internal combustion engine automobile technologies: A 25-year life cycle and fleet impact assessment. *Energy* **31**, 2064-2087, doi:http://dx.doi.org/10.1016/j.energy.2005.09.011 (2006).
  - 14 Ellis, M. W., Von Spakovsky, M. R. & Nelson, D. J. Fuel cell systems: efficient, flexible energy conversion for the 21st century. *Proceedings of the IEEE* **89**, 1808-1818, doi:10.1109/5.975914 (2001).
  - 15 Steele, B. C. H. & Heinzl, A. Materials for fuel-cell technologies. *Nature* **414**, 345-352 doi:10.1038/35104620 (2001).
  - 16 Chalk, S. G. & Miller, J. F. Key challenges and recent progress in batteries, fuel cells, and hydrogen storage for clean energy systems. *Journal of Power Sources* **159**, 73-80, doi:10.1016/j.jpowsour.2006.04.058 (2006).
  - 17 Cheng, X., Shi, Z., Glass, N., Zhang, L., Zhang, J., Song, D., Liu, Z.-S., Wang, H. & Shen, J. A review of PEM hydrogen fuel cell contamination: Impacts, mechanisms, and mitigation. *Journal of Power Sources* **165**, 739-756, doi:10.1016/j.jpowsour.2006.12.012 (2007).
  - 18 Sundmacher, K., Schultz, T., Zhou, S., Scott, K., Ginkel, M. & Gilles, E. D. Dynamics of the direct methanol fuel cell (DMFC): experiments and model-based analysis. *Chemical Engineering Science* **56**, 333-341, doi:10.1016/s0009-2509(00)00233-5 (2001).
  - 19 Dusastre, V. & Kilner, J. A. Optimisation of composite cathodes for intermediate temperature SOFC applications. *Solid State Ionics* **126**, 163-174, doi:10.1016/s0167-2738(99)00108-3 (1999).
  - 20 Huijsmans, J. P. P., van Berkel, F. P. F. & Christie, G. M. Intermediate temperature SOFC – a promise for the 21st century. *Journal of Power Sources* **71**, 107-110, doi:10.1016/s0378-7753(97)02789-4 (1998).

- 21 Frackowiak, E. & Béguin, F. Carbon materials for the electrochemical storage of energy in capacitors. *Carbon* **39**, 937-950, doi:10.1016/s0008-6223(00)00183-4 (2001).
- 22 Hirsch, A. The era of carbon allotropes. *Nat Mater* **9**, 868-871 doi:10.1038/nmat2885 (2010).
- 23 Kroto, H. W., Heath, J. R., O'Brien, S. C., Curl, R. F. & Smalley, R. E. C60: Buckminsterfullerene. *Nature* **318**, 162-163 doi:10.1038/318162a0 (1985).
- 24 Terrones, M., Botello-Méndez, A. R., Campos-Delgado, J., López-Urías, F., Vega-Cantú, Y. I., Rodríguez-Macías, F. J., Elías, A. L., Muñoz-Sandoval, E., Cano-Márquez, A. G., Charlier, J.-C. & Terrones, H. Graphene and graphite nanoribbons: Morphology, properties, synthesis, defects and applications. *Nano Today* **5**, 351-372, doi:10.1016/j.nantod.2010.06.010 (2010).
- 25 Geng, D., Wu, B., Guo, Y., Huang, L., Xue, Y., Chen, J., Yu, G., Jiang, L., Hu, W. & Liu, Y. Uniform hexagonal graphene flakes and films grown on liquid copper surface. *Proceedings of the National Academy of Sciences* **109**, 7992-7996, doi:10.1073/pnas.1200339109 (2012).
- 26 Dong, Y.-P., Zhang, J., Ding, Y., Chu, X.-F. & Zhang, W.-B. Enhanced Cathodic Electrogenerated Chemiluminescence of Luminol at a Graphene Modified Electrode in Neutral Solution. *Journal of The Electrochemical Society* **159**, H692-H696, doi:10.1149/2.020208jes (2012).
- 27 Park, S. & Ruoff, R. S. Chemical methods for the production of graphenes. *Nat Nano* **4**, 217-224 doi:10.1038/nnano.2009.58 (2009).
- 28 Balandin, A. A., Ghosh, S., Bao, W., Calizo, I., Teweldebrhan, D., Miao, F. & Lau, C. N. Superior Thermal Conductivity of Single-Layer Graphene. *Nano Letters* **8**, 902-907, doi:10.1021/nl0731872 (2008).
- 29 Service, R. F. Carbon Sheets an Atom Thick Give Rise to Graphene Dreams. *Science* **324**, 875-877, doi:10.1126/science.324\_875 (2009).
- 30 Lee, C., Wei, X., Kysar, J. W. & Hone, J. Measurement of the Elastic Properties and Intrinsic Strength of Monolayer Graphene. *Science* **321**, 385-388, doi:10.1126/science.1157996 (2008).
- 31 Hummers, W. S. O., R. E. Preparation of Graphitic Oxide. *J. Am. Chem. Soc.* **80**, 1339-1339. doi:10.1021/ja01539a017 (1985).

- 32 Schniepp, H. C., Li, J.-L., McAllister, M. J., Sai, H., Herrera-Alonso, M., Adamson, D. H., Prud'homme, R. K., Car, R., Saville, D. A. & Aksay, I. A. Functionalized Single Graphene Sheets Derived from Splitting Graphite Oxide. *The Journal of Physical Chemistry B* **110**, 8535-8539, doi:10.1021/jp060936f (2006).
- 33 Novoselov, K. S., Jiang, D., Schedin, F., Booth, T. J., Khotkevich, V. V., Morozov, S. V. & Geim, A. K. Two-dimensional atomic crystals. *Proceedings of the National Academy of Sciences of the United States of America* **102**, 10451-10453, doi:10.1073/pnas.0502848102 (2005).
- 34 Boukhvalov, D. W., Katsnelson, M. I. & Lichtenstein, A. I. Hydrogen on graphene: Electronic structure, total energy, structural distortions and magnetism from first-principles calculations. *Physical Review B* **77**, 035427 doi:10.1103/PhysRevB.77.035427 (2008).
- 35 Niyogi, S., Bekyarova, E., Itkis, M. E., McWilliams, J. L., Hamon, M. A. & Haddon, R. C. Solution Properties of Graphite and Graphene. *Journal of the American Chemical Society* **128**, 7720-7721, doi:10.1021/ja060680r (2006).
- 36 A.A. Balandin, S. G., W. Bao, I. Calizo, D. Teweldebrhan, F. Miao, C.N. Lau. Superior Thermal Conductivity of Single-Layer Graphene. *Nano Letters* **8**, 902 doi:10.1021/nl0731872 (2008).
- 37 Zhao, X., Zhang, Q., Chen, D. & Lu, P. Enhanced Mechanical Properties of Graphene-Based Poly(vinyl alcohol) Composites. *Macromolecules* **43**, 2357-2363, doi:10.1021/ma902862u (2010).
- 38 Bolotin, K. I., Sikes, K. J., Jiang, Z., Klima, M., Fudenberg, G., Hone, J., Kim, P. & Stormer, H. L. Ultrahigh electron mobility in suspended graphene. *Solid State Communications* **146**, 351-355, doi:10.1016/j.ssc.2008.02.024 (2008).
- 39 Srinivas, G., Zhu, Y., Piner, R., Skipper, N., Ellerby, M. & Ruoff, R. Synthesis of graphene-like nanosheets and their hydrogen adsorption capacity. *Carbon* **48**, 630-635, doi:10.1016/j.carbon.2009.10.003 (2010).
- 40 Antoine, O., Bultel, Y. & Durand, R. Oxygen reduction reaction kinetics and mechanism on

- platinum nanoparticles inside Nafion® . *Journal of Electroanalytical Chemistry* **499**, 85-94, doi:10.1016/s0022-0728(00)00492-7 (2001).
- 41 A. Damjanovic, V. B. ELECTRODE KINETICS OF OXYGEN REDUCTION ON OXIDE-FREE PLATINUM ELECTRODES. *Electrochim. Acta* **12**, 615 doi: http://dx.doi.org/10.1016/0013-4686(67)8030-8 (1967).
- 42 Sepa, D. B., Vojnovic, M. V. & Damjanovic, A. Reaction intermediates as a controlling factor in the kinetics and mechanism of oxygen reduction at platinum electrodes. *Electrochimica Acta* **26**, 781-793, doi:10.1016/0013-4686(81)90037-2 (1981).
- 43 Hummers, W. S. & Offeman, R. E. Preparation of Graphitic Oxide. *Journal of the American Chemical Society* **80**, 1339-1339, doi:10.1021/ja01539a017 (1958).
- 44 Hsieh, C.-T. & Lin, J.-Y. Fabrication of bimetallic Pt–M (M=&#xa0;=&#xa0;Fe, Co, and Ni) nanoparticle/carbon nanotube electrocatalysts for direct methanol fuel cells. *Journal of Power Sources* **188**, 347-352, doi:10.1016/j.jpowsour.2008.12.031 (2009).
- 45 Jeon, T.-Y., Yoo, S. J., Cho, Y.-H., Lee, K.-S., Kang, S. H. & Sung, Y.-E. Influence of Oxide on the Oxygen Reduction Reaction of Carbon-Supported Pt–Ni Alloy Nanoparticles. *The Journal of Physical Chemistry C* **113**, 19732-19739, doi:10.1021/jp9076273 (2009).
- 46 Antoine, O. & Durand, R. RRDE study of oxygen reduction on Pt nanoparticles inside Nafion® : H<sub>2</sub>O<sub>2</sub> production in PEMFC cathode conditions. *Journal of Applied Electrochemistry* **30**, 839-844, doi:10.1023/a:1003999818560 (2000).
- 47 Wang, G.-j., Gao, Y.-z., Wang, Z.-b., Du, C.-y., Wang, J.-j. & Yin, G.-p. Investigation of PtNi/C anode electrocatalysts for direct borohydride fuel cell. *Journal of Power Sources* **195**, 185-189, doi:10.1016/j.jpowsour.2009.06.080 (2010).
- 48 Lin, J.-J. & Chen, Y.-M. Amphiphilic Properties of Poly(oxyalkylene)amine-Intercalated Smectite Aluminosilicates. *Langmuir* **20**, 4261-4264, doi:10.1021/la0362775 (2004).
- 49 Wang, Z.-C., Ma, Z.-M. & Li, H.-L. Functional multi-walled carbon nanotube/polysiloxane composite films as supports of PtNi alloy nanoparticles for methanol electro-oxidation. *Applied Surface Science* **254**, 6521-6526, doi:10.1016/j.apsusc.2008.04.017 (2008).

- 50 Wang, G., Yang, J., Park, J., Gou, X., Wang, B., Liu, H. & Yao, J. Facile Synthesis and Characterization of Graphene Nanosheets. *The Journal of Physical Chemistry C* **112**, 8192-8195, doi:10.1021/jp710931h (2008).
- 51 Pawelec, B., Damyanova, S., Arishtirova, K., Fierro, J. L. G. & Petrov, L. Structural and surface features of PtNi catalysts for reforming of methane with CO<sub>2</sub>. *Applied Catalysis A: General* **323**, 188-201, doi:10.1016/j.apcata.2007.02.017 (2007).
- 52 A. K. Shukla, K. V. R., R. Manoharan, P. R. Sarode, S. Vasudevan. Preparation and Characterization of Platinized-Carbon Hydrogen Anodes for Alkali and Acid Fuel Cells. *Phys. Chem.* **89**, 1261 doi: 10.1002/bbpc.19850891205 (1985).
- 53 Hüfner, S. & Wertheim, G. K. Core-line asymmetries in the x-ray-photoemission spectra of metals. *Physical Review B* **11**, 678-683 doi: 10.1103/PhysRevB.11.678 (1975).
- 54 Hammond, J. S. & Winograd, N. XPS spectroscopic study of potentiostatic and galvanostatic oxidation of Pt electrodes in H<sub>2</sub>SO<sub>4</sub> and HClO<sub>4</sub>. *Journal of Electroanalytical Chemistry and Interfacial Electrochemistry* **78**, 55-69, doi:10.1016/s0022-0728(77)80422-1 (1977).
- 55 Park, K.-W., Choi, J.-H. & Sung, Y.-E. Structural, Chemical, and Electronic Properties of Pt/Ni Thin Film Electrodes for Methanol Electrooxidation. *The Journal of Physical Chemistry B* **107**, 5851-5856, doi:10.1021/jp0340966 (2003).
- 56 Seger, B. & Kamat, P. V. Electrocatalytically Active Graphene-Platinum Nanocomposites. Role of 2-D Carbon Support in PEM Fuel Cells. *The Journal of Physical Chemistry C* **113**, 7990-7995, doi:10.1021/jp900360k (2009).
- 57 Mayrhofer, K. J. J., Strmcnik, D., Blizanac, B. B., Stamenkovic, V., Arenz, M. & Markovic, N. M. Measurement of oxygen reduction activities via the rotating disc electrode method: From Pt model surfaces to carbon-supported high surface area catalysts. *Electrochimica Acta* **53**, 3181-3188, doi:10.1016/j.electacta.2007.11.057 (2008).
- 58 Pozio, A., De Francesco, M., Cemmi, A., Cardellini, F. & Giorgi, L. Comparison of high surface Pt/C catalysts by cyclic voltammetry. *Journal of Power Sources* **105**, 13-19, doi:10.1016/s0378-7753(01)00921-1 (2002).

- 59 Schmidt, T. J., Gasteiger, H. A., Stäb, G. D., Urban, P. M., Kolb, D. M. & Behm, R. J. Characterization of High-Surface-Area Electrocatalysts Using a Rotating Disk Electrode Configuration. *Journal of The Electrochemical Society* **145**, 2354-2358, doi:10.1149/1.1838642 (1998).
- 60 Gottesfeld, S., Raistrick, I. D. & Srinivasan, S. Oxygen Reduction Kinetics on a Platinum RDE Coated with a Recast Nafion Film. *Journal of The Electrochemical Society* **134**, 1455-1462, doi:10.1149/1.2100689 (1987).
- 61 Wang, X., Li, W., Chen, Z., Waje, M. & Yan, Y. Durability investigation of carbon nanotube as catalyst support for proton exchange membrane fuel cell. *Journal of Power Sources* **158**, 154-159, doi:10.1016/j.jpowsour.2005.09.039 (2006).
- 62 Miah, M. R. & Ohsaka, T. Kinetics of oxygen reduction reaction at tin-adatoms-modified gold electrodes in acidic media. *Electrochimica Acta* **54**, 5871-5876, doi:10.1016/j.electacta.2009.05.045 (2009).
- 63 Stephen Treimer, A. T., Dennis C. Johnson. A Consideration of the Application of Koutecký-Levich Plots in the Diagnoses of Charge-Transfer Mechanisms at Rotated Disk Electrodes. *Electroanalysis* **14**, 165-171 doi: 10.1002/1521-4109(200202) (2002).
- 64 Gurau, B. & Smotkin, E. S. Methanol crossover in direct methanol fuel cells: a link between power and energy density. *Journal of Power Sources* **112**, 339-352, doi:10.1016/s0378-7753(02)00445-7 (2002).
- 65 Aricò, A. S., Cretì, P., Antonucci, P. L. & Antonucci, V. Comparison of Ethanol and Methanol Oxidation in a Liquid-Feed Solid Polymer Electrolyte Fuel Cell at High Temperature. *Electrochemical and Solid-State Letters* **1**, 66-68, doi:10.1149/1.1390638 (1998).
- 66 Yang, H., Coutanceau, C., Léger, J.-M., Alonso-Vante, N. & ClaudeLamy. Methanol tolerant oxygen reduction on carbon-supported Pt-Ni alloy nanoparticles. *Journal of Electroanalytical Chemistry* **576**, 305-313, doi:10.1016/j.jelechem.2004.10.026 (2005).
- 67 Wu, H., Wexler, D. & Liu, H. Pt-Ni/C catalysts using different carbon supports for the

- cathode of the proton exchange membrane fuel cell (PEMFC). *Materials Chemistry and Physics* **136**, 845-849, doi:10.1016/j.matchemphys.2012.08.007 (2012).
- 68 Borup, R., Meyers, J., Pivovar, B., Kim, Y. S., Mukundan, R., Garland, N., Myers, D., Wilson, M., Garzon, F., Wood, D., Zelenay, P., More, K., Stroh, K., Zawodzinski, T., Boncella, J., McGrath, J. E., Inaba, M., Miyatake, K., Hori, M., Ota, K., Ogumi, Z., Miyata, S., Nishikata, A., Siroma, Z., Uchimoto, Y., Yasuda, K., Kimijima, K.-i. & Iwashita, N. Scientific Aspects of Polymer Electrolyte Fuel Cell Durability and Degradation. *Chemical Reviews* **107**, 3904-3951, doi:10.1021/cr050182i (2007).
- 69 Chen, Y., Wang, J., Liu, H., Li, R., Sun, X., Ye, S. & Knights, S. Enhanced stability of Pt electrocatalysts by nitrogen doping in CNTs for PEM fuel cells. *Electrochemistry Communications* **11**, 2071-2076, doi:10.1016/j.elecom.2009.09.008 (2009).

## 국문 요약문

### 그라핀 지지체를 사용한 백금-니켈 나노입자 합금의 산소 환원 반응(ORR) 능력

고분자 전해질 막 연료전지 (PEMFC)는 화학 에너지로부터 직접 전기 에너지를 발생시켜 기존 내연 기관보다 높은 효율을 가진다는 점에서 널리 연구되어 왔다. 하지만 연료전지는 상업화를 이루기 위해 많은 도전 과제를 품고 있다. 높은 가격 절감과 촉매 활성 촉진이 연료전지 상업화를 위한 주된 과제에 해당한다. 높은 가격의 백금이 연료전지 양극과 음극에 모두 사용되기 때문에, 가격 절감을 위해 백금의 양을 감소하는 것이 요구된다. 백금과 Fe, Co, 그리고 Ni과 같은 이차 전이 금속과의 합금은 백금 촉매의 양을 줄일 수 있고 연료전지 가격 절감을 기대할 수 있다. 촉매 활성 부분에서는 백금-M(M=Fe, Co, Ni, etc.) 합금뿐만 아닌 촉매의 탄소 지지체 역시 고려되어야 한다. 카본 블랙(Vulcan XC-72) 및 탄소나노튜브(CNT)와 같은 흑연 물질은 연료전지 촉매의 탄소 지지체로 널리 사용되어 왔다. 또한 그라핀은 이것이 가지는 높은 전기 전도도와 넓은 표면적, 열적 안정성 등의 이유로 발견 이래 금속 나노입자 지지체로써 폭넓게 사용되었다.

가격 절감과 높은 산소환원반응(ORR) 능력을 위해 백금-니켈 합금 촉매를 합성 하였고 촉매의 ORR 능력을 평가하였다. 음극에서의 ORR은 양극에 비해 활성이 낮으며 이것은 연료전지 성능의 막대한 영향을 미치기 때문에 음극에서의 촉매 ORR 능력 향상은 필수적이다. 그라핀을 지지체로 사용한 백금-니켈 나노입자 합금 촉매는 상업용 Pt/C 촉매와 카본 블랙(Vulcan XC-72) 및 탄소나노튜브(CNT)를 지지체로 사용한

백금-니켈 나노입자 합금 촉매와도 비교 분석 하였다. 세가지 다른 전극촉매는 모두 연료전지 성능에 우수한 4전자 반응을 따랐으며 그 중 그래핀을 지지체로 사용한 백금-니켈 나노입자 합금 촉매가 ORR면에 있어 가장 높은 활성을 보였다. 또한 그래핀을 지지체로 사용한 백금-니켈 나노입자 합금 촉매는 메탄올의 내성면에 있어서도 가장 높은 내성을 가진 촉매로 평가되었다. 백금-니켈 나노입자 합금 촉매들은 주사전자현미경, 투과전자현미경, X선 회절법, 그리고 X선 광전자 분광법과 같은 물리적-화학적 기법들을 이용하여 분석 되었다. 백금-니켈 나노입자 합금 촉매의 전기화학적 특성은 CV, LSV, RDE, 그리고 RRDE와 같은 기법들을 이용하여 비교 분석 하였다. 본 연구에서는 다양한 탄소 지지체와 함께 백금-니켈 나노입자 합금 촉매의 구체적인 특성과 ORR 활성에 대하여 논의될 것이다.

핵심어 : 연료전지, 그래핀, 백금-니켈 합금 촉매, 산소 환원 반응(ORR) 능력

## Acknowledgements

First of all I want to thanks to my professor, Dr. Shanmugam Sangaraju. I appreciate his teaching and concern for 2 years. And it was very happy to spend almost 2 years with, my friends, Kriangsak and Jakkid. Also I appreciate to Prakash and Dr. Sahu. I hope you to having good memories of Korea.

2011년 2월 처음 만나 지금까지 마치 가족처럼 옆에서 서로를 응원해주고 뒤에서 든든한 버팀목이 되어준 우리 연구실 가족과 동기들께 감사의 말씀을 드립니다. 못난 lab 오빠 만나 고생시켜 더욱 미안한 가영이, 더 어른스럽고 부지런한 용이, 연구 외에도 배울게 참 많은 태은이 모두 사랑하고 고맙습니다.

언제나 친형처럼 옆에서 잘 챙겨준 일연이형과 영준이형에게 감사 드립니다. 특히 2년 동안 철없는 룸메이트를 만나 아빠의 마음으로 모든걸 챙겨주고 걱정해주고 함께 울고 웃어 주었던 순욱이형에게 감사 드립니다. 또한 언제나 함께 해준 모든 2012년 1기 동기들 인혜, 준교형, 승효, 하영이, 유미, 동환이형, 동휘, 은영이에게 감사의 말씀을 전합니다. 대구로 다시 돌아와 대학원 생활을 한다 하였을 때 응원해주고 연락해 주었던 대학 동기와 친구들에게도 감사합니다.

좋은날, 슬픈날, 힘든날을 막론하고 전화한 통화에 달려와준 오랜 친구 의환이, 명현이, 지용이, 호준이, 우석이. 사랑하고 고맙다.

마지막으로 제가 이날까지 여기 있어서 이 모든걸 가능하게 해주신 저희 부모님과 누나. 믿음과 사랑으로 언제나 옆에서 함께 있어주셔서 항상 감사 드리고 사랑합니다.

